Analysis of an Artificial Tailplane Icing Flight Test of a High-Wing, Twin-Engine Aircraft

by

SHEHZAD M. SHAIKH

Presented to the Faculty of the Graduate School of

The University of Texas at Arlington in Partial Fulfillment

of the Requirements

for the Degree of

MASTER OF SCIENCE IN AEROSPACE ENGINEERING

THE UNIVERSITY OF TEXAS AT ARLINGTON
May 2016

ACKNOWLEDGEDGMENTS

"In the Name of Allah, the Most Gracious, the Most Merciful"

First, I am very thankful to ALLAH for giving me the capability and patience to complete the project.

I am grateful to my supervising professor Dr. Robert "Bob" Mullins for his guidance, kind support and faith in me. I am also very thankful to Drs. Dudley Smith and Don Wilson for being the part of the thesis committee member.

It was a great opportunity, and both a challenging and a pleasant experience for me to be a student of the Aerospace Engineering department to complete this thesis at the University of Texas at Arlington.

I am truly grateful to my loving and caring parents and family who helped, supported, guided, and prayed for me to have success in my present endeavor. And last but not the least I am grateful to my friends for motivating me and supporting me during this project.

April 29, 2016

ABSTRACT

ANALYSIS OF AN ARTIFICIAL TAIL PLANE ICING FLIGHT TEST OF A HIGH-WING, TWIN ENGINE AIRCRAFT

Shehzad M Shaikh, MS

The University of Texas at Arlington, 2016

Supervising Professor: Dr. Baxter R. Mullins, Jr.

The US Air Force Flight Test Center (AFFTC) conducted a civilian, Federal Aviation Administration (FAA) sponsored, evaluation of tailplane icing of a twin-turboprop business transport at Edwards Air Force Base. The flight test was conducted to evaluate ice shape growth and extent of ice on the tailplane for specific weather conditions of Liquid Water Content (LWC), droplet size, and ambient temperature.

This work analyzes the flight test data comparing the drag for various tailplane icing conditions with respect to a flight test verified calibrated aircraft model.

Although less than a third of the test aircraft was involved in the icing environment, the results of this analysis shows a significant increase in the

aircraft drag with respect to the LWC, droplet size, and ambient temperature.

TABLE OF CONTENTS

TABLE OF CONTENTS (cont.)

TABLE OF CONTENTS (cont.)

LIST OF ILLUSTRATIONS

LIST OF ILLUSTRATIONS (cont.)

LIST OF ILLUSTRATIONS (cont.)

LIST OF TABLES

NOMENCLATURE

FAA	Federal Aviation Administration
DC	Direct Current
AC	Alternate Current
MVD	Mean Volumetric Diameter
LWC	Liquid Water Content
OAT	Outside air temperature
TIT	Turbine inlet temperature
RPM	Revolutions per minute
V_{KIAS}	Indicated Air Speed
V_{TAS}	True Air Speed
SHP	Shaft Horse Power

Chapter 1 Introduction

In the 1980's and 1990's several civil and commercial turboprop aircraft were involved in accidents in which airframe icing played a major role. Petty and Floyd[1] presented a statistical review of U.S. aviation airframe icing accidents between 1982 and 2000 at an American Meteorological Society meeting in which they reported 583 accidents with 80.8% of the accidents related to general aviation aircraft and 17.6% Part 135 aircraft. Commuter and many medium and small businesses use twin-engine reciprocating and turboprop powered aircraft that generally operate at altitudes below 25,000 feet in a region of the atmosphere with the highest probability for exposure to icing[2]. The normal operating envelope for these aircraft requires an "all-weather" capability including flight into known icing. This increases the likelihood of accidents resulting from changes in the performance of the aerodynamic surfaces when ice is present. Ongoing icing research has resulted in the increased availability of data on the aerodynamic performance of the individual components of an airplane and of the total aircraft. These studies have shown that icing can cause a significant increase in drag and a significant reduction in maximum lift. Wing-tail interaction with tailplane icing can result in the phenomena of horizontal tailplane stall[3].

This research is a continuation of analytical and experimental work examining the effects of icing on the aerodynamic performance of a horizontal stabilizer due to residual ice formation. Initial research was proposed by Dr. Kenneth Korkan at Texas A&M University to examine two-dimensional airfoil shapes of three sections, a NACA 23012, a NACA 64A415-mod, and a NACA 64A010-mod. NASA's LEWICE[4] was used to predict ice shapes after which the forward section of the ice was removed to simulate the action of a deicing boot in shedding of ice[5]. An experimental program was conducted to examine the effects of simulated ice shapes and shedding for the three sections. The models were based on a 24% scale of a typical turboprop business class airplane. The results showed a maximum lift coefficient reduction of 40-60% and increase in drag of 300-500 percent[6].

As the airfoils were small and the lift and drag results were affected by the low Reynolds number, a larger model was proposed using a two-dimensional flapped airfoil with a NACA 64A010-mod airfoil section. The model was scaled to be about 57% of a typical business-class turboprop horizontal tailplane chord with a 40% flap. The experiments again examined the effects of simulated leading edge ice and ice shedding. The tests were conducted for angles of attack between ±6 degrees for flap deflections between -28 degrees and +12 degrees. Test results showed an

increase in the profile drag between 300% and 400%. The residual ice shapes disrupted the chordwise pressure distribution. This change in chordwise pressure distribution alters the flap hinge moment which in turn affects the flap trim requirements. Chordwise location of the residual ice shape with respect to the leading-edge of the airfoil showed significant changes in laminar bubble separation extent and reattachment with significant separation without reattachment occurring for ice shapes nearer the leading edge. The aerodynamic performance of the 57% scaled model compares very favorably with full scale data[7].

Although the 57% flapped airfoil offered a good representation of the full-scale horizontal stabilizer a follow-on experimental program was conducted using a modified full-scale horizontal stabilizer from a representative business-class turboprop aircraft. Wind tunnel tests were conducted to systematically document the experimentally observed effects of generic ice formation and its partial rejection on the aerodynamic characteristics of a full-scale, 3-dimensional, “as manufactured” horizontal tail assembly. The airfoil section of the test device was a NACA 64A010-mod which matched the airfoil section of the previous two tests. Test configurations included a clean, as manufactured, horizontal empennage with a naturally weathered pneumatic deicing boot and a new pneumatic deicing boot, and various combinations of simulated light icing and heavy

icing configurations with residual ice ridges formed aft of the deicing boot after activation. The residual shapes were based on a LEWICE model developed by Dr. Korkan. The extent of boot coverage in percent chord and flap position were also evaluated. Experimentally obtained test data indicate that even light icing conditions result in a significant increase in the minimum drag coefficient (C_{D_0}), while larger protuberances simulating various ice shapes resulted in more than 300 percent increase in drag for zero flap conditions. Maximum lift coefficient ($C_{L_{max}}$) was significantly reduced with the stall angle of attack reduced from 22 degrees to 14 degrees. Finally, there was a slight reduction in the lift curve slope (C_{L_α}) probably due to leading-edge flow separation[8].

The current work is a follow-on to the previous analytical and experimental work. Fortunately, an icing flight test was conducted by the United States Air Force at the Air Force Flight Test Center, 6510 Test Wing at Edwards Air Force Base in California using a modified tanker (S/N 55-3128) to provide artificial icing. In addition to the Air Force Icing Tanker, a fully instrumented Mitsubishi MU-2B-60 was available for in-flight icing tests and a Learjet Model 36 was available to be used as a chase and safety aircraft and was also for measuring the cloud stream characteristics before and after the in-flight icing tests to verify properties.

Chapter 2 Test Plan

This test was designed to verify the growth and extent of ice aft of the active boot for specific weather conditions of liquid water content, droplet size, and ambient temperature. In addition, activation of the pneumatic boots in the condition was planned to verify ice shedding and the rejection shapes remaining after boot operation.

Nine test points were planned as shown in Table 1. The required separation distance between the tanker and the test aircraft and instrumented chase aircraft was determined by the icing parameters to meet the test point conditions. The test duration for each point could vary depending on the ice conditions experienced by the test aircraft.

TABLE 1. TEST DATA POINTS

Test Point	Desired MVD (microns)	Required LWC (g/m^3)	TOAT (C)	TIME (min)	AIRSPEED (KIAS)
1	20	0.2	-5	15	190
2	20	0.4	-5	15	190
3	20	0.6	-5	15	190
4	40	0.2	-5	15	190
5	40	0.4	-5	15	190
6	40	0.6	-5	15	190
7	40	0.8	-5	15	190
8	30	0.8	-5	15	150
9	30	0.6	-5	15	170

Notes: (1) Test point #8 is with test aircraft One Engine Inoperative (OEI).
(2) Test point #9 is with flaps 20.
(3) Airspeed may range between 150 and 200 KIAS based on flight condition.
(4) The test data point may be reduced if ice thickness limits are reached.

Planned Test Procedure

The test altitude will depend on achieving the required OAT and will be determined by the AFFTC flight test (icing specialist) engineer. The instrumented chase plane will enter the cloud produced behind the tanker to record and provide information to the flight test engineer on board the tanker for calibration of the required conditions. If changes to the water flow rate or to aircraft separation distance are required, the instrumented chase plane will drop out of the cloud and then repeat the calibration once adjustments have been made.

Once the instrumented chase plane has confirmed the ice conditions specified for the test point have been achieved, the chase plane departs the stream and the test aircraft then enters the cloud in the same position that the instrumented chase plane vacated. The test aircraft positions itself such that exposure to the cloud is limited to the left side of the aircraft. Instrumentation on board the tanker monitors the separation distance to ensure that it is maintained. Left engine Torque, Turbine Inlet Temperature (TIT), percent RPM, Airspeed, and aircraft TRIM is monitored by the test aircraft crew. A sudden loss in or rapid decrease in airspeed, engine power, or excessive trim requirements results in rapid termination of the test.

Ice accrues on the left main wing and left tailplane until it reaches a thickness of approximately 0.125 inches on the tailplane. At this point, the

test aircraft clears the stream and the pilot stabilizes the aircraft and activates the leading edge pneumatic boots. The test aircraft pilots evaluate the aircraft performance degradation before re-entering the ice cloud. The ice will then be allowed to accrue on the left wing and left tailplane until it reaches a thickness of approximately 0.25 inches on the tailplane or 0.5 inches on the main wing. At this point, the test aircraft again departs the ice cloud and the pilot again activates the pneumatic boots. The test aircraft pilot further evaluates the aircraft performance degradation. If the specific icing condition and the ice thickness limits have not been reached, the test duration can be extended as appropriate. When the test point has been terminated, the remaining ice Is allowed to sublimate or shed before proceeding to the next test point. Additional test points will repeat the procedure with a higher Liquid Water Content (LWC) and/or higher Medium Volumetric Diameter (MVD)[9].

Test Objectives

The objective of this test is to (1) examine ice accretion on the aircraft resulting from droplets greater than 20 microns, (2) evaluate performance degradation of the test aircraft due to ice accretion, (3) evaluate performance degradation of the subject aircraft due to partial rejection of accumulated ice, and (4) examine horizontal tail icing characteristics during One Engine Inoperative (OEI) condition.

Chapter 3 TEST EQUIPMENT AND INSUMENTATION

Icing Tanker

The U.S. Air Force modified a NKC-135A tanker aircraft (S/N 55-3128) to provide artificial icing and/or rain cloud conditions for in-flight aircraft testing. The general requirement for rain and ice testing was in AF 80-31, “All-Weather Qualification Program for Air Force Systems and Material.” MIL-STD-210C, “Climate Extremes for Military Equipment” and MIL-STD-810D, “Environmental Test Methods” were the driving factors in creating the system for in-flight testing. The modified aircraft has been used to test more than 30 military and civil aircraft.

The tanker can carry 2000 lbs of demineralized water and provide a spray diameter of about 7 feet at the expected separation distance of 50 feet. The icing tanker can provide flows of up to 55 gallons per minute through the boom and nozzle array. The circular array used for this test has a maximum diameter of 44 inches with the smallest ring being only 12 inches in diameter. The spray is emitted from one-hundred nozzle elements. Figure 1 shows the U.S. Air Force Icing Tanker in formation with the test aircraft. A complete description may be found in reference 9, “The Air Force Flight Test Center Artificial Icing and Rain Testing Capability Upgrade Program.”

Figure 1. United States Air Force Icing Tanker SN 55-3128 in formation with the Mitsubishi MU-2B-60 test aircraft in the water stream.

Chase and Safety Aircraft

A Gates Learjet Model 36 was used as a chase aircraft and performed additional functions including measurements of the water flow emitted from the spray nozzle, photographic and videotaping of the test aircraft wing and horizontal stabilizer. The instruments about the Learjet

collected parameters such as Liquid Water Content (LWC), Mean Volumetric Diameter (MVD), Relative Humidity (RH), and Outside Air Temperature (OAT). Video equipment was provided not only for the Chase, but for the tanker which provided a frontal view of the test aircraft wing and tailplane ice accretion and shedding. The chase video system was used to monitor the ice accretion and shedding on the fuselage, wing, horizontal tail and vertical tail. Upper and lower wings and horizontal stabilizer were monitored and as determined by the chase crew close-up video and stills taken. All video was time stamped.

The instrumented Learjet performed cloud calibration using two laser spectrometers, a Johnson and Williams's Liquid Water Content probe, and instruments for ambient air temperature, dew point, and airspeed. A Forward Scattering Spectrometer (FSSP) and a Cloud Particle Spectrometer (CPS) were used to measure droplet size and Liquid Water Content (LWC). The chase aircraft performed horizontal and vertical sweeps of the cloud to compare to "FAA FAR Part 25, Appendix C"[10]. Figure 2 provides a photograph from the icing tanker of the Learjet during a calibration sweep of the cloud. The calibration instrument can be observed under the Learjet's left wing.

Figure 2. Gates Learjet Model 36 chase aircraft during a calibration sweep of the cloud being emitted from the icing tanker nozzle.

Flight Test Aircraft

The flight test aircraft is a Mitsubishi MU-2B-60. The horizontal stabilizer uses a 64A010-mod airfoil similar to the experimental wind tunnel models used in previous testing. It is a twin-engine, high-wing, utility aircraft with a circular cross section, retractable tricycle undercarriage and is fitted

with large wingtip tanks. The MU-2B-60 is a long body derivative with excellent speed performance. The aircraft has a high wing loading (65 pounds per square foot) and uses modified 6-series airfoils to improve performance. The aircraft uses full-span double-slotted flaps to improve landing performance and as a result uses spoilers for roll control. A highly modified inverted, 6-series airfoil section with a leading edge droop is used for the horizontal stabilizer to improve low-speed landing characteristics. The aircraft is certified for flight into known icing and has pneumatic boots on the leading edge of the wings, horizontal stabilizer, and vertical stabilizer. It also has various flight equipment protected by heating. The aircraft has a wing span of 37.083 feet, wing area of 178.143 square feet, and a chord of 5.0459 feet. The aircraft is powered by two Garrett TPE331-10-501M engines rated at 715 SHP. The weight is in the 11,000-pound class. A three-view drawing is provided in Figure 3 and a photograph in Figure 4.

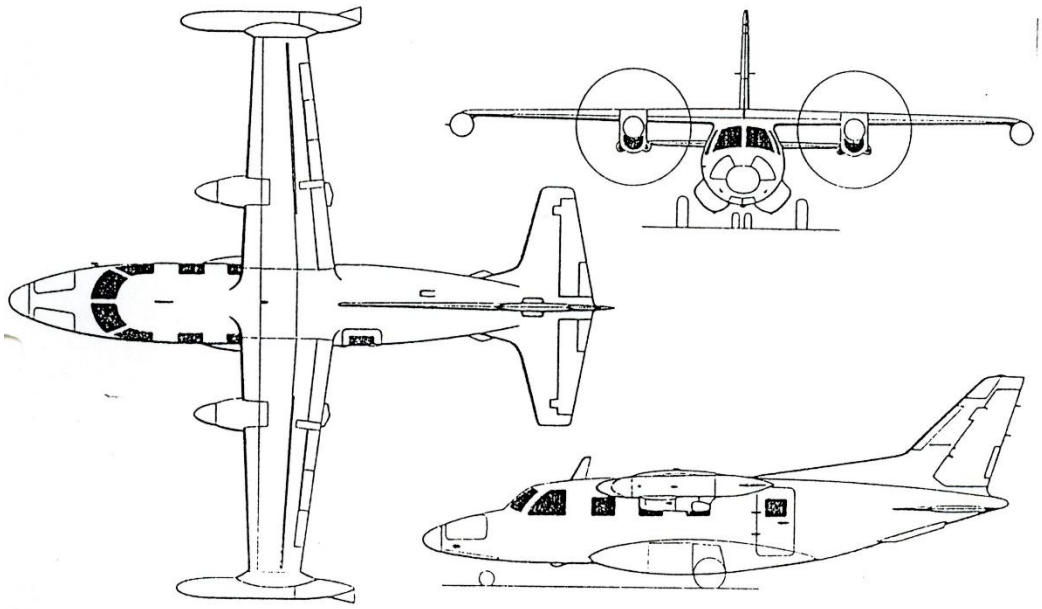

Figure 3. Mitsubishi MU-2B-60 3-view Drawing.

Figure 4. Mitsubishi MU-2B-60 Flight Test Aircraft in the cloud stream

Flight Test Aircraft Instrumentation

Kohlman Systems Research supplied the data acquisition system for the test aircraft to record engine performance parameters; flight control positions; air data, including temperature from a total temperature fitted under the right wing of the test aircraft. Kohlman Systems collected data from the test vehicle and the chase aircraft and provided the data in a combined data package. A list of the items recorded is provided in Table 2.

In addition to the instrument package a number of video cameras were mounted on the flight test aircraft to record the top and bottom of the horizontal stabilizer and a number of hand-held video cameras to record the underside of the wing. Additional video cameras were mounted in the cockpit to observe to instrument panel and engine instruments[9].

TABLE 2. FLIGHT AIRCRAFT INSTRUMENTAION DATA LIST

ITEM	DEFINITION
BLKCNT	Time Slice Counter
IRIGB_TIME	IRIG-B Time (seconds)
AX	Linear Acceleration (g) Positive Forward
AY	Lateral Acceleration (g) Positive Out Right Wing
AZ	Vertical Acceleration (g) Positive Down
PITCH_RATE	Pitch Rate (deg/sec) Positive Nose Up
ROLL_RATE	Roll Rate (deg/sec) Positive Right Wing Down
YAW_RATE	Yaw Rate (deg/sec) Positive Nose Right
PITCH_ACC	Pitch Acceleration (deg/sec/sec) Positive Nose Up
ROLL_ACC	Roll Acceleration (deg/sec/sec) Positive Right Wing Down
YAW_ACC	Yaw Acceleration (deg/sec/sec) Positive Nose Right
PITCH_ATT	Pitch Attitude (deg) Positive Nose Up
ROLL_ATT	Roll Attitude (deg) Positive Right Wing Down
TORQUE_L	Left Engine Torque (%)
TORQUE_R	Right Engine Torque (%)
EGT_L	Left Exhaust Gas Temperature (deg C)
EGT_R	Right Exhaust Gas Temperature (deg C)
RPM_L	Left Engine Speed (%)
RPM_R	Right Engine Speed (%)
ELE_DEF	Elevator Deflection (deg) Positive Trailing Edge Down
ELE_TAB	Elevator Tab Deflection (deg) Positive Trailing Edge Down
STATIC_PX	Static Pressure (psf)
DIFF_PX	Differential Pressure (psf)
TAT	Total Air Temperature (deg K)
H_IND	Pressure Altitude (ft)
KIAS	Indicated Airspeed (kt)
MACH_IND	Indicated Mach Number
QBAR_IND	Indicated Dynamic Pressure (psf)
IRIG_B_RAW	Raw IRIG Signal, Binary Coded Decimal (not Meaningful)
CG_LONG_FS	Longitudinal Center Of Gravity, Fuselage Station (IN)
CG_PCT_MAC	Longitudinal Center Of Gravity, % Mean Aerodynamic Chord
FUEL_USED	Fuel Used (lb)
AC_WEIGHT	Aircraft Weight (lb)

TABLE 2 FLIGHT AIRCRAFT INSTRUMENTAION LIST (Cont.)

ITEM	DEFINITION
FUEL_WT	Fuel On Board Weight (lb)
MVD	Median Volumetric Diameter, (micron)
LWC	Liquid Water Content, (Gram/cubic Meter)
CLOUD_TEMP	Ice Cloud Static Air Temperature (deg C)

.

CHAPTER 4 FLIGHT TESTS

The flight tests were conducted at Edwards Air Force Base over a five-day period and accumulated a total of 12-flight hours, two more hours of testing than originally allocated. Figure 5 shows an annotated flight card used to conduct the flight tests. In preparing for the tests, multiple flight cards were created so that flight tests could be changed based on flight-by-flight evaluation of the conditions. As such, multiple flight cards were prepared for each day. Only those flight test numbers in yellow were actually conducted

Tests conducted

Day 1 of the tests was used to familiarize the flight crews with their aircraft and to conduct practice runs in flying formation with the icing tanker. The test aircraft conducted calibration runs with flaps up (clean) configuration and flaps set at 20 degrees.

Day 2 through Day 5 conducted a number of flights obtaining data in both clean and flaps 20 configurations. These runs examined the aircraft icing accumulation for various liquid water contents and mean variable diameter super-cooled water droplets at temperatures near -5 Celsius.

ICING FLIGHT TEST CARD

	FLT CARD NO.	FLGT	TEST	RUN	KIAS	FREEZING LEVEL	OAT (°C)	TEMP LEVEL	FLAPS	LWC	MVD	NOTES
4-Feb-93	1	1	1	1.1	190		-5.0 (+0/-5)		CLEAN	N/A	N/A	FAMILIARIZATION - PERFORMANCE BASELINE (CLEAN)
	1	1	1	1.2	155		-5.0 (+0/-5)		20	N/A	N/A	FAMILIARIZATION - TORQUE VS AIRSPEED PROFILE
	1	1	1	1.3	160		-5.0 (+0/-5)		As Reqd OEI	N/A	N/A	
9-Feb-93	4	2	1	2A	190	7000	-5.0 (+0/-5)	9200/10200	CLEAN	0.2	20	
	4	2	1	3A	190		-5.0 (+0/-5)		CLEAN	0.4	30	NOT RUN
	4	2	1	4A	190		-5.0 (+0/-5)		CLEAN	0.6	40	NOT RUN
	4A	2	1	2A	155		-5.0 (+0/-5)		20	0.2	20	NOT RUN
	4A	2	1	3A	155		-5.0 (+0/-5)		20	0.4	30	NOT RUN
	4A	2	1	4A	155		-5.0 (+0/-5)		20	0.6	40	NOT RUN
	4B	2	1	8C	155		-5.0 (+0/-5)		20	0.2	20	NOT RUN
	4B	2	1	9C	155		-5.0 (+0/-5)		20	0.4	30	NOT RUN
	4B	2	1	10C	155		-5.0 (+0/-5)		20	0.6	40	NOT RUN
	5	2	1	5B	190		-5.0 (+0/-5)		CLEAN	0.2	20	NOT RUN
	5	2	1	6B	190		-5.0 (+0/-5)		CLEAN	0.4	30	NOT RUN
	5	2	1	7B	190		-5.0 (+0/-5)		CLEAN	0.6	40	NOT RUN
10-Feb-93	4A	3	1	2A	190		-5.0 (+0/-5)		CLEAN	0.2	20	NOT RUN
	4A	3	1	3A	190		-5.0 (+0/-5)		CLEAN	0.4	30	NOT RUN
	4A	3	1	4A	190	6500	-5.0 (+0/-5)	10500	CLEAN	0.6	40	
	4B	3	1	8C	155		-5.0 (+0/-5)	11500	20	0.2	20	
	4B	3	1	9C	155		-5.0 (+0/-5)		20	0.4	30	NOT RUN
	4B	3	1	10C	155		-5.0 (+0/-5)		20	0.6	40	NOT RUN
11-Feb-93	4B	2	1	8C	155		-5.0 (+0/-5)		20	0.2	20	NOT RUN
	4B	2	1	9C	155		-5.0 (+0/-5)		20	0.4	30	NOT RUN
	4B	2	1	10C	155		-5.0 (+0/-5)	10300	20	0.6	40	
	5	2	1	5B	190		-5.0 (+0/-5)		CLEAN	0.2	20	NOT RUN
	5	2	1	6B	190		-5.0 (+0/-5)		CLEAN	0.4	30	NOT RUN
	5	2	1	7B	190		-5.0 (+0/-5)	10300	CLEAN	0.6	40	
12-Feb-93	5	2	1	5B	160		-5.0 (+0/-5)		CLEAN	0.2	20	NOT RUN
	5	2	1	6B	160		-5.0 (+0/-5)		CLEAN	0.4	30	NOT RUN
	5	2	1	7B	160	7300	-5.0 (+0/-5)	10900	CLEAN	0.6	40	

Figure 5. Flight Test Card used in the icing flight tests – only.
The run numbers in yellow were actually conducted.

Test Matrix

Figure 6 provides a copy of the flight text matrix as executed. The data shown in the matrix shows the flight number, flight test card run or point as recorded, time and duration of the test run, airspeed (KIAS), outside air temperature (OAT), liquid water content (LWC), and mean variable diameter (MVD) of the water droplet. Note that the point number contains the flight card number and the MVD of the water droplet, i.e., a 4A.50 would be flight card number 2A with a MVD of 50 microns. The comment column provides a description of the events and when they took place.

Flight Test Process

The three aircraft crews would meet at a preflight meeting to discuss the day's flight plan which included choosing the flight cards for the day. Once the preflight briefing was completed, the aircraft would takeoff and fly to the appropriate test area at Edwards Air Force Base, where the icing tanker would climb to an appropriate altitude to meet the outside air temperature of -5 Celsius and setup a "race-track" orbit at the preselected airspeed. The flight test aircraft would climb to altitude to cold soak the aircraft as the temperature of the aircraft exterior had to be at the same temperature as the outside air temperature. Flight instruments were

	FLT	/ PT	TIME (ZULU)	KCAS+2=KIAS	OAT	LWC	MVD	COMMENTS
8-Feb-93	1	/ 1.1	18:05	230 - 145	0° C	N/A	N/A	PERFORMANCE BASELINE AND PILOT FAMILIARZATION
	1	/ 1.2	18:45	150 - 92		N/A	N/A	FLIGHT: DELETED RUN 1.3 DUE TO TIME DATE: 3 FEB 93
9-Feb-93	2	/ 2A.25	18:25	189	-5°C	0.29	19.8	CALIBRATION (CAL), LAUNCG MU-2
			18.56	192	-6°C	0.216	21.5	CAL
			19:06	196	-5.5			START FIRST 1/4" INCREMENT
			19:13	192	-6.0			DEPART CLOUD, ONE BOOT ACTIVATION
			19:25	190	-6.5	0.259	21.5	CAL
	2	/ 2A.5	19:35	196	-5.4			START 1/2" INCREMENT
			19:46	190	-7.2			DEPART CLOUD, TWO BOOT ACTIVATIONS
			19:59	194	-8.1	0.225	22	CAL, ICING ON ARRAY, RTB
10-Feb-93	3	/ 4A.25	18:18	192	-6.9	0.657	2.96	CAL
			18:24	192	-6.1			START FIRST 1/4" INCREMENT
			18:28	193	-6.0			DEPART CLOUD, TWO BOOT ACTIVATIONS, NO EL RES ICE
			18:40	190	-8.0	0.559	30	CAL
	3	/ 4A.50	18:47	190	-7.0			START 1/2" INCREMENT, 1/2 TO 3/4 LE ACCUMULATIONS ON ELEVATOR, AERODYNAMIC SHEDDING
			18:53	190.5	-7.2			DEPART CLOUD, TWO BOOT ACTIVATIONS, 80-90% SHED ON FIRST ACTIVATION
			19:07	190	-7.5	0.60	30.3	CAL
	3	/ 4A-75	19:14	190	-6.5			START 3/4" INCREMENT, LARGE BUILD-UP ON PITOT TUBE
			19:28	190	-6.4			DEPART CLOUD, ONE BOOT ACTIVATION
			19:43	192	-7.5	0.694	30	CAL
	3	/ 4A.10	19:47	200	-8.0			START 1" INCREMENT
			20:06	194	-5.5			DEPART CLOUD, ≈ 10 KIAS AIRSPEED DECREASE BEFORE BOOT ACTIVATION, GOOG SHED AFTER ACTIVATION
	3	/ 8C.25	20:28	194	-7.0	0.229	20.9	CAL
			20:32	194	-6.5			START 1/4" INCREMENT
			20:42	193	-6.1			DEPART CLOUD, SLOW FOR FLAPS 20°
			20:50	N/A				ONE BOOT ACTIVATION, NEGLIGABLE AMOUNT OF ICE REMAINS ON ELEVATOR LE BOOT.

Figure 6. Flight test matrix for the first three days of testing.

	FLT	/ PT	TIME (ZULU)	KCAS+2=KIAS	OAT	LWC	MVD	COMMENTS
11-Feb-93	4	/ 7B.25	19:24	178	-5.5	0.611	.31.8	CAL (MU-2 COLD SOAKED)
			19:36	182	-5.5			START 1/4" INCREMENT
			19:41	180	-5.8			DEPART CLOUD
	4	/ 7B.50	19:56.15	186	-5.7			START 1/2" INCREMENT, SOME AERO SHEDDING
			20:10.42	185	-5.2			DEPART CLOUD, TIME LIMIT REACHED
	4	/ 7B.25	20:16	176	-4	0.695	32.9	CAL
			20:18	176	-5.4			START 1/4" INCREMENT
			27:13	176	-5.9			DEPART CLOUD, CLEAN SHED ON FIRST ACTIVATION
	4	/ 7B.50	34:31	173	-5.8			STAR 1/2" INCREMENT
			20:49.49	180	-5.2			DEPART CLOUD, TIME LIMIT REACHE, ICE RIDGES UNDER MAIN WING BEHIND BOOT, DID NOT SHED PRIOR TO NEXT POINT.
	4	/ 7B.50+	20:56.30	172	-5.8			START NEXT 15 MINUTE POINT
			21:03.50	169	-4.5			DEPART CLOUD, 2 TO 3" ICE RIDGES UNDER MAIN WING BEHIND BOOT, AREA BEHIND ELEV BOOT CLEAN
	4	/ 10C.25	21:42.52	176	-5.2	0.747	25	CAL
			21:44.00	176	-5.4			START 1/4" INCREMENT, ICE BEHIND MAIN WING BOOTS, LOWER
			21:52.00	177	-5.1			DEPART CLOUD, SLOW FOR 20^{O} FLAP
	4	/ 10C.50	22:03:40	176	-5.6			START 1/2" INCREMENT
			22:14:34	176	-5.0			DEPART CLOUD, SLOW FOR 20^{o} FLAP
			22:15:28	176	-5.1	0.588	23	CAL, RTB BINGO ON MU-2 FUEL
12-Feb-93	5	/ 7B.25	20:06.40	170	-6.5	0.785	47	CAL (MU-2 COLD SOAKED)
			20:28	164	-4.7			START 1/4" INCREMENT
			20:31	164	-6.3			DEPART CLOUD
	5	/ 7B.50	20:38	168				START 1/2" INCREMENT
			20:45	168				DEPART CLOUD, CLEAN TAIL SHED
			20:47.37	168	-5.0	0.72	36	CAL
	5	/ 7B.75	20:50.50	164	-4.5			START 3/4" INCREMENT
			21:03	164				DEPART CLOUD, NO AERO SHEDDING VISABLE
	5	/ 7B.10	21:14	164.5	-4.1	0.58	35	CAL
			21:17	161	-3.8			START 1" INCREMENT, CLASSICAL GLAZE (MUSHROOM) FORM
			21:32	161				DEPART CLOUD, CLEAN TAIL SHED, ACCEL 20 KIAS AFTER SHED
			21:39	165	-3.9	0.654	32	CAL, RTB, TETS COMPLETE

Figure 7. Flight test matrix for the last two days of testing.

checked out and calibrated. The chase aircraft carried equipment to measure the liquid water content (LWC), mean volume diameter (MVD), relative humidity (RH), and temperature of the water cloud produced by the icing tanker.

Water Stream Coverage

The cloud, or water stream, is produced by a circular frame containing 100 nozzles with 49 providing a water stream while the remaining 51 being used for anti-icing using aircraft engine bleed air[10]. The nozzle array has five rings (Figure 8) with the smallest being twelve inches in diameter, and the largest ring is forty-four inches in diameter.

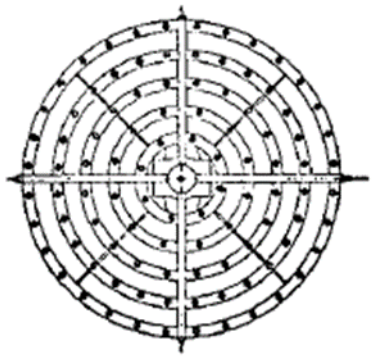

Figure 8. U.S. Air Force Icing Tanker' circular icing array.

Since the super-cooled water cloud produced at the circular area was only forty-four inches, only a small portion of the test aircraft could be covered with the spray. The cloud expanded from the diameter of the array

to about seven feet. Ice would be allowed to accrue on the left main wing and left tailplane. The approximate coverage is shown in Figure 9.

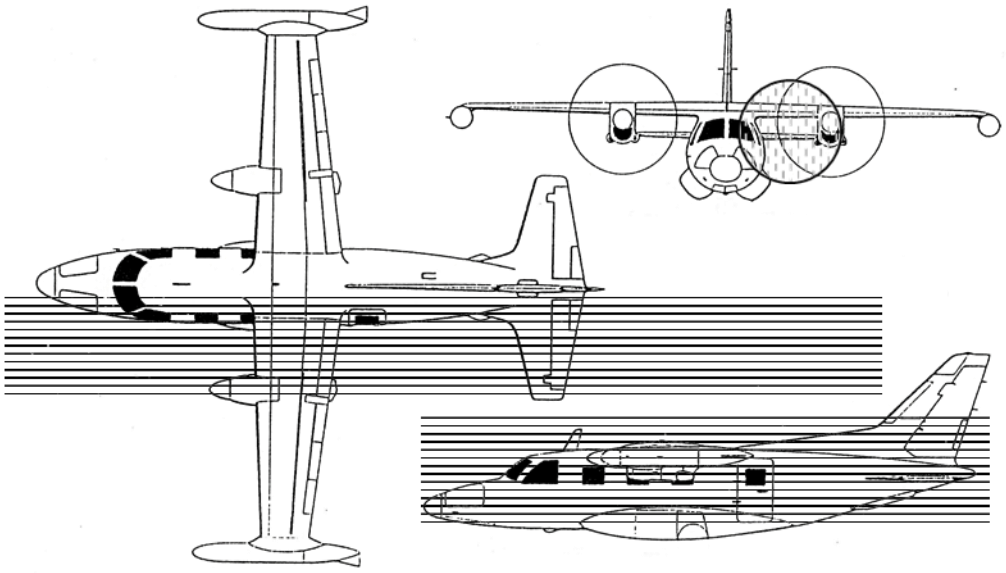

Figure 9. Cloud stream is focused on the left-side of the test aircraft and has a diameter at the aircraft is approximately 7 feet 10 inches in diameter.

Test Procedure as Conducted

The test altitude depended on achieving the required OAT and was determined by the flight test engineer on board the icing tanker.

The instrumented chase plane entered the cloud produced behind the tanker to record and provide information to the flight test engineer onboard the tanker for calibration of the required conditions. If changes to the water flow rate or aircraft separation distance are required, the

instrumented plane would drop out of the cloud and then repeat the calibration once adjustments had been made.

Once the instrumented chase plane confirmed the ice conditions specified for the test point were achieved, the chase plane departed the stream and the test aircraft entered the cloud in the same position as the instrumented chase plane vacated. The test aircraft positioned itself such that exposure to the cloud is limited to the left side to the maximum extent possible. Instrumentation on board the tanker monitored the separation distance to ensure it was maintained. Engine torque, turbine inlet temperature, percent RPM, airspeed, and aircraft trim will be monitored by the test aircraft crew and flight test engineer. Consideration was given to possible ice formation and ingestion effects. A sudden loss or rapid decrease in airspeed, engine power loss, or excessive trim requirements will result in test point termination.

Ice was accrued on the aircraft horizontal stabilizer in one-quarter inch increments. At each point the pilot cleared the cloud, stabilized, and activate the pneumatic boots. Personal and video observations of the icing and deicing were conducted from the tanker and the chase plane. In addition, the pilot evaluated the performance of the aircraft before reentering the cloud for the next cycle of ice accretion. If the time limit is reached, without achieving the specific icing condition described in detail on

the flight card procedures, the test duration was extended as appropriate. If the time limit was reached and the icing effects were achieved, then the next test point on the daily flight card was performed.

CHAPTER 5. DATA COLLECTED

The data collected included photographic, video, and instrument data from the icing tanker, the chase plane, and icing test aircraft. In addition, sketches of the ice formation on the flight test vehicle were constructed showing relative location and extent of the ice accumulation.

Cloud Data Measurements (Chase) Aircraft

The Gates Learjet flew with an instrument under the right wing to measure the stream data. The cloud calibration was performed with an instrument consisting of two laser spectrometers, a Johnson and William's Liquid Water Content (LWC) probe, and indication for ambient air temperature, dew point, and airspeed. A Forward Scattering Spectrometer Probe (FSSP) and the Cloud Particle Spectrometer (CPS) were used to measure droplet size (MVD) and liquid water content (LWC).

Droplet Distribution

Droplet distribution was provided as a set of tables for each test condition. The initial table was a summary of the conditions for a given test point. In particular, a test point may contain one or more conditions based on the number of icing cycles the test aircraft conducted for a given flight card. A sample of a summary chart is provided in Figure 10 and an individual flight condition test point is provided in Figure 11.

TEST POINT SUMMARY OF AVERAGE CONDITIONS FOR INDICATED TIME PERIODS
FLIGHT: 209 DATE: 93/2/9

RUN #	TIME PERIOD PST	ALT kft	TAS kts	TEM C	RH %	PKLWC g/m3	ALWC g/m3	MVD um	RATE gpm	REMARKS
1	102736-102748	9.1	215	-6	79	0.39	0.29	22	3.3	system check 0.2 g/m3
2	105838-105847	9.2	215	-4	47	0.26	0.16	24		pre cal 0.2 g/m3
3	105952-110002	9.2	226	-4	44	0.26	0.14	23		pre cal 0.2 g/m3
4	112650-112657	9.1	218	-4	40	0.27	0.15	24	3.8	after 1st shed
5	112736-112744	9.3	219	-5	16	0.30	0.15	22		after 1st shed
	SWEEP THROUGH CLOUD AFTER COMPLETION OF TEST AT 0.2 g/m3 WAS NOT OBTAINED									
	THE SWEEP MISSED THE CLOUD!!!!!!									
6	120132-120141	10.9	230	-8	13	0.38	0.26	24		setup for 0.4 g/m3

ALWC = LWC OF THE AVERAGE DSD OF SAMPLES WHERE LWC/PKLWC >= 0.05.
MVD = MVD OF THE AVERAGE DSD " " " " " " " .

ALT, TAS, TEM, AND RH REPRESENT AVERAGES OVER INDICATED TIME PERIOD.
NOTE:!!!!!!!!!!!! DEW POINT SENSOR ACTED STRANGE.
IGNORE RH FOR ENTIRE FLIGHT!!!!!!!!!!
DON TAKEUCHI

SEE FILE NAMED F209.LST FOR TIME LISTINGS FOR ALL RUN #'s.
RUN # 2 & 3 TAKEN BEFORE MU2 ENTERED THE CLOUD.
RUN # 4 & 5 TAKEN AFTER THE INITIAL ICE SHED.
A SWEEP WAS MADE AFTER THHE COMPLETION OF THE TEST AT 0.2 G/M3 BUT I BELIEVE WE MISSED THE CLOUD.
RUN # 6 WAS A MEAUREMENT TAKEN FOR THE 0.4 G/M3 POINT BUT WE HAD TO RTB SHORTLY AFTER WITHOUT THE MU2 GOING INTO THE CLOUD.

Figure 10. An example of a test point summary average conditions for an indicated time period for flight 209.

AVERAGE DROPSIZE DISTRIBUTION
DATE: 93/2/9 RUN NUMBER: 1 TIME PERIOD(PST): 102736- 102748

PALT(kft): 9.12 TAS(kts): 215 TEM(C): -6 RH(%): 79
LWC(g/m3): 0.29 MVD(um): 22

Di (um)	Nd (/m3/um)	LWCd (g/m3/um)	CLWC (%)
3	1.4191E+07	2.0062E-04	0.21
6	2.3373E+07	2.6435E-03	2.97
9	2.0379E+07	7.7787E-03	11.10
12	1.2359E+07	1.1182E-02	22.78
15	5.6520E+06	9.9880E-03	33.22
18	3.3113E+06	1.0111E-02	43.79
21	1.7376E+06	8.4259E-03	52.59
24	1.0394E+06	7.5234E-03	60.45
27	5.4692E+05	5.6366E-03	66.34
30	2.7406E+05	3.8744E-03	70.39
33	1.0837E+05	2.0391E-03	72.52
36	7.8917E+04	1.9279E-03	74.53
39	2.0152E+04	6.2591E-04	75.19
42	1.0192E+04	3.9537E-04	75.60
45	1.2801E+03	6.1079E-05	75.67
60	8.8055E+03	9.9588E-04	83.47
80	3.2985E+03	8.8426E-04	89.63
100	1.2446E+03	6.5165E-04	94.17
120	4.0160E+02	3.6336E-04	96.70
140	1.7363E+02	2.4946E-04	98.44
160	4.3347E+01	9.2964E-05	99.09
180	0.0000E+00	0.0000E+00	99.09
200	0.0000E+00	0.0000E+00	99.09
220	6.9021E+00	3.8481E-05	99.35
240	7.5101E+00	5.4360E-05	99.73
260	4.1688E+00	3.8364E-05	100.00
280	0.0000E+00	0.0000E+00	100.00
300	0.0000E+00	0.0000E+00	100.00

AVERAGE DROPSIZE DISTRIBUTION
DATE: 93/2/9 RUN NUMBER: 2 TIME PERIOD(PST): 105838- 105847

Figure 11. Average droplet size data table.

Figure 12a shows a typical distribution of super-cooled water droplets in the cloud stream as measured from the chase aircraft instrumentation. Figure 12b shows the distribution of the liquid water content of the cloud.

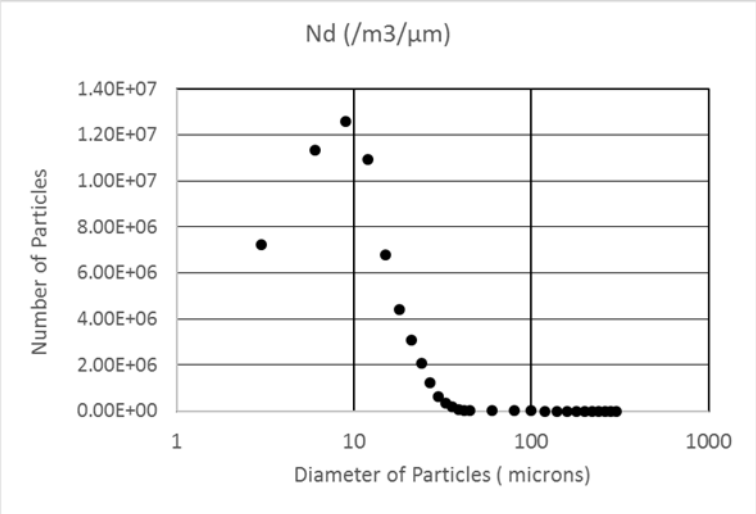

(a) Particle distribution in cloud stream.

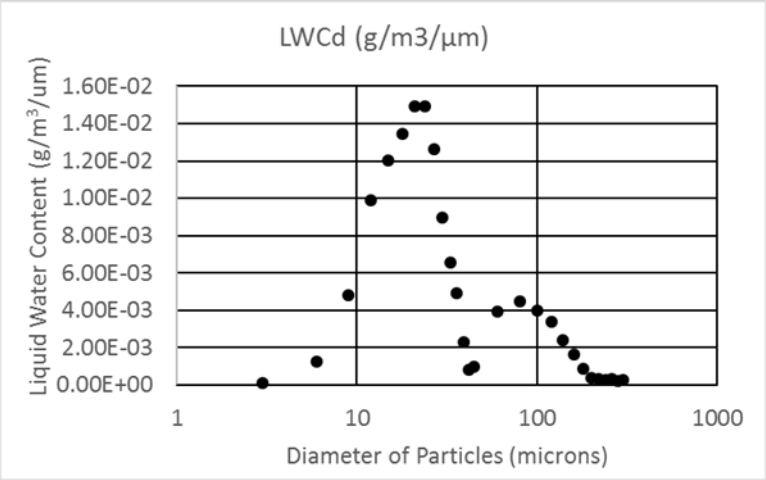

(b) Liquid Water Content distribution content in the cloud.

Figure 12. An example of the particle distribution and Liquid Water Content in cloud stream at -5 C, at 10,570 feet, 100% relative humidity for an average 0.78 g/m3 LWC and a MDV 64 microns.

Flight Test Vehicle Data

The flight test aircraft carried a calibrated instrument package provided by Kolhman Systems Research as previously described in Chapter 3. The data from the system was provided as text files as a function of time with one set of data points listed every tenth of a second for the duration of a test segment. The data was collected at a rate of 10 samples per second is shown in Table 2. Figure 13 shows a sample of the data provided. These data files are easily loaded into a spreadsheet or a program like MATLAB®. These data files are of a time window and do not necessarily contain the sequence of an icing sequence but of the time period beginning near the time the test aircraft pulled out of the cloud.

In addition to the data files a set of graphics where provided for each data set as described in Figure 6, “Flight test matrix for the last two days of testing.” Figure 14 provides a sample of the description page and the graphics page for test condition 2A, Run 009.

.

Input	file	name	=	MU20032A006A													
Converted:	22-Feb-93	12:11:00															
Date:	30-Aug-93	15:19:10															
BLKCNT	IRIGB_TIME	AX	AY	AZ	PITCH_RATE	ROLL_RATE	YAW_RATE	PITCH_ACC	ROLL_ACC	YAW_ACC	PITCH_ATT	ROLL_ATT	TORQUE_L	TORQUE_R	EGT_L	EGT_R	RPM_L
(DEG)		(G)	(G)	(G)	(DEG/SEC)	(DEG/SEC)	(DEG/SEC)	(DEG/S/S)	(DEG/S/S)	(DEG/S/S)	(DEG)	(DEG)	(%)	(%)	(DEG C)	(DEG_C)	(%)
1	68482	7.13E-02	2.00E-02	-0.9051	-0.544493	0.372987	-3.05E-02	3.01426	-2.47279	0.405822	3.02469	0.804465	49.6516	50.1591	496.771	495.066	100.381
2	68482.1	2.51E-02	-1.76E-02	-0.8518	-0.192729	8.44E-02	1.69E-02	4.11946	-5.97587	0.202911	2.9345	0.804465	49.0486	49.8634	496.771	494.815	100.353
3	68482.3	5.80E-02	7.82E-03	-0.8883	0.41699	-1.02178	1.69E-02	4.42088	-2.26672	0.101464	2.96456	0.760444	48.9625	49.779	497.022	495.066	100.381
4	68482.4	6.01E-02	5.97E-02	-0.8967	0.839105	-0.44464	4.06E-02	1.80855	-0.206066	-0.202911	3.11488	0.672393	48.7902	49.5256	497.022	495.066	100.353
5	68482.5	6.60E-02	-4.89E-03	-0.9612	0.839105	-1.06988	-3.05E-02	-1.90902	-2.26669	-0.60875	3.17501	0.452285	48.9625	49.6945	496.771	494.312	100.353
6	68482.6	5.75E-02	2.37E-02	-1.0005	0.393541	-0.973686	-0.101499	-2.61235	-1.03033	-0.202928	3.23514	0.452285	49.307	50.1591	496.52	494.563	100.353
7	68482.7	3.30E-02	-1.55E-02	-0.9893	0.229383	-1.31036	-7.78E-02	-1.80855	-3.91525	0.304375	3.2652	0.188148	49.5654	50.5814	496.27	494.061	100.381
8	68482.9	4.15E-02	3.38E-02	-1.0314	-2.86E-02	-1.8875	-3.05E-02	-2.31092	-2.26672	0.101464	3.23514	5.61E-02	50.0392	50.7503	496.27	494.312	100.381
9	68483	6.28E-02	3.64E-02	-1.0678	-0.309985	-1.83941	-5.41E-02	-2.21045	-1.44246	-0.507302	3.23514	-0.164033	50.1253	50.5391	496.27	494.312	100.41
10	68483.1	7.76E-02	1.79E-02	-0.9977	-0.544493	-2.22417	-0.148862	-1.30617	2.47279	-0.304375	3.11488	-0.384148	49.9961	50.6658	496.019	494.312	100.353
11	68483.2	7.66E-02	-1.65E-02	-0.9725	-0.614844	-1.26226	-0.125181	-0.502367	5.35771	0.507302	3.05475	-0.604256	50.2114	50.7503	496.019	494.312	100.353

RPM_R	ELE_DEF	ELE_TAB	STATIC_PX	DIFF_PX	TAT	H_IND	KIAS	MACH_IND	QBAR_IND	IRIG_B_RAW	CG_LONG_FS	CG_PCT_MAC	FUEL_USED	AC_WEIGHT	FUEL_WT	MVD	LWC	CLOUD_TEMP
(%)	(DEG)	(DEG)	(PSF)	(PSF)	(DEG K)	(FT)	(KT)		(PSF)	(BCD_SEC)	(INCHES)	(%)	(LB)	(LB)	(LB)	(UM)	(G/M**3)	(DEG C)
100.092	-3.11221	6.4884	1501.04	124.932	274.828	9200.73	190.129	0.33989	121.385	4.20E+08	196.59	30.0976	231	11090	2134	23	0.15	-4
100.092	-3.2186	6.51912	1501.04	125.283	274.787	9200.73	190.39	0.340354	121.717	4.20E+08	196.59	30.0976	231	11090	2134	23	0.15	-4
100.092	-3.0056	6.4884	1500.48	126.511	274.828	9210.27	191.303	0.342033	122.875	4.20E+08	196.59	30.0976	231	11090	2134	23	0.15	-4
100.064	-3.0056	6.4884	1500.48	126.16	274.828	9210.27	191.042	0.341571	122.544	4.20E+08	196.59	30.0976	231	11090	2134	23	0.15	-4
100.092	-3.11221	6.4884	1501.04	125.283	274.828	9200.73	190.39	0.340354	121.717	4.20E+08	196.59	30.0976	231	11090	2134	23	0.15	-4
100.092	-2.6845	6.45768	1501.04	124.756	274.787	9200.73	189.998	0.339658	121.22	4.20E+08	196.59	30.0976	231	11090	2134	23	0.15	-4
100.12	-2.89878	6.4884	1501.04	124.756	274.787	9200.73	189.998	0.339658	121.22	4.20E+08	196.59	30.0976	231	11090	2134	23	0.15	-4
100.092	-2.79175	6.42694	1501.59	124.756	274.828	9191.19	189.998	0.339597	121.221	4.20E+08	196.59	30.0976	231	11090	2134	23	0.15	-4
100.092	-2.89878	6.42694	1501.59	124.23	274.828	9191.19	189.605	0.3389	120.723	4.20E+08	196.59	30.0976	231	11090	2134	23	0.15	-4
100.092	-3.0056	6.4884	1501.59	123.879	274.787	9191.19	189.342	0.338434	120.392	4.20E+08	196.59	30.0976	231	11090	2134	23	0.15	-4
100.092	-3.11221	6.45768	1501.04	123.528	274.745	9200.73	189.079	0.338028	120.059	4.20E+08	196.59	30.0976	231	11090	2134	23	0.15	-4

Figure 13. Example of data file provided from the data acquisition system of the flight test aircraft.

.

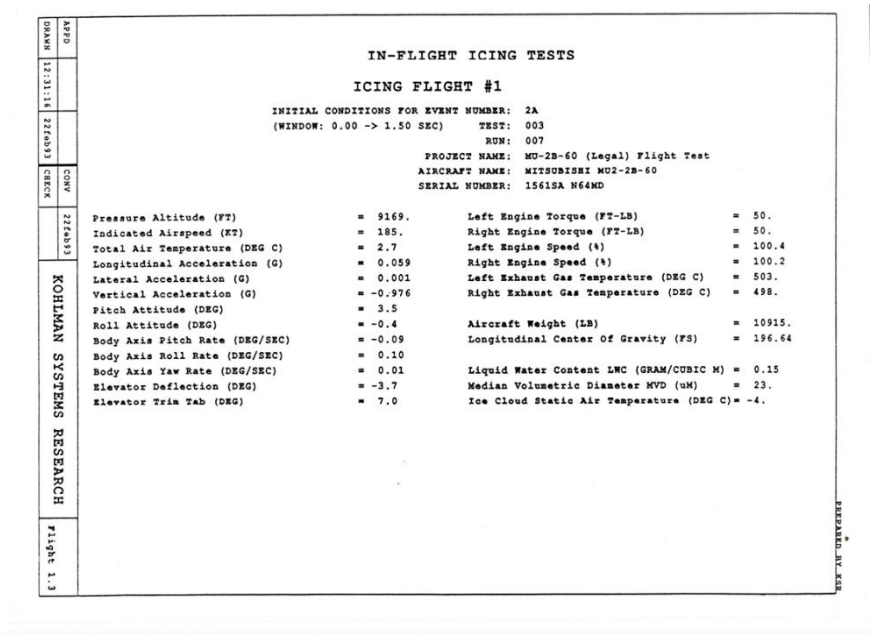

IN-FLIGHT ICING TESTS

ICING FLIGHT #1

INITIAL CONDITIONS FOR EVENT NUMBER: 2A
(WINDOW: 0.00 -> 1.50 SEC) TEST: 003
RUN: 007
PROJECT NAME: MU-2B-60 (Legal) Flight Test
AIRCRAFT NAME: MITSUBISHI MU2-2B-60
SERIAL NUMBER: 1561SA N64MD

Pressure Altitude (FT)	= 9169.	Left Engine Torque (FT-LB)	= 50.
Indicated Airspeed (KT)	= 185.	Right Engine Torque (FT-LB)	= 50.
Total Air Temperature (DEG C)	= 2.7	Left Engine Speed (%)	= 100.4
Longitudinal Acceleration (G)	= 0.059	Right Engine Speed (%)	= 100.2
Lateral Acceleration (G)	= 0.001	Left Exhaust Gas Temperature (DEG C)	= 503.
Vertical Acceleration (G)	= -0.976	Right Exhaust Gas Temperature (DEG C)	= 498.
Pitch Attitude (DEG)	= 3.5		
Roll Attitude (DEG)	= -0.4	Aircraft Weight (LB)	= 10915.
Body Axis Pitch Rate (DEG/SEC)	= -0.09	Longitudinal Center Of Gravity (FS)	= 196.64
Body Axis Roll Rate (DEG/SEC)	= 0.10		
Body Axis Yaw Rate (DEG/SEC)	= 0.01	Liquid Water Content LWC (GRAM/CUBIC M)	= 0.15
Elevator Deflection (DEG)	= -3.7	Median Volumetric Diameter MVD (uM)	= 23.
Elevator Trim Tab (DEG)	= 7.0	Ice Cloud Static Air Temperature (DEG C)	= -4.

DRAWN 12:31:16 22feb93 APPD CHECK CONV 22feb93 KOHLMAN SYSTEMS RESEARCH Flight 1.3

(a)

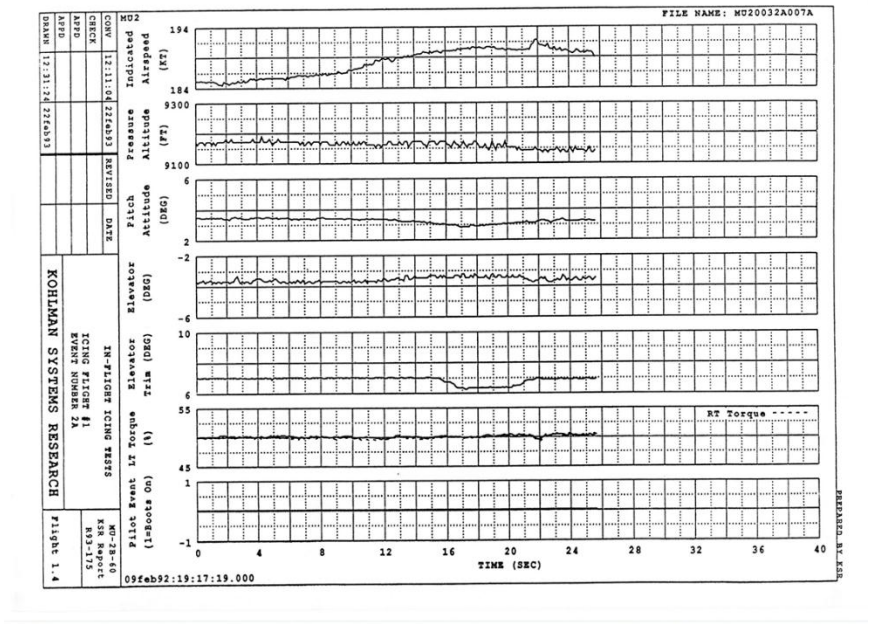

(b)

Figure 14. Sample output provided in the flight test data package.

CHAPTER 6 CALCULATION MODELS

Method for Determining Drag

For a given flight card data point, a set of data as defined in Table 2, Flight Aircraft Instrumentation Data List, was generated every tenth of a second for a time window. Each test aircraft variable was smoothed by non-phase shifting, fifth-order Butterworth filter[14] and the smoothed data was used to determine drag assuming performance model was acceptable for performing the necessary calculations. The performance model assumes the flight test aircraft maintains a relatively stable flight attitude[15].

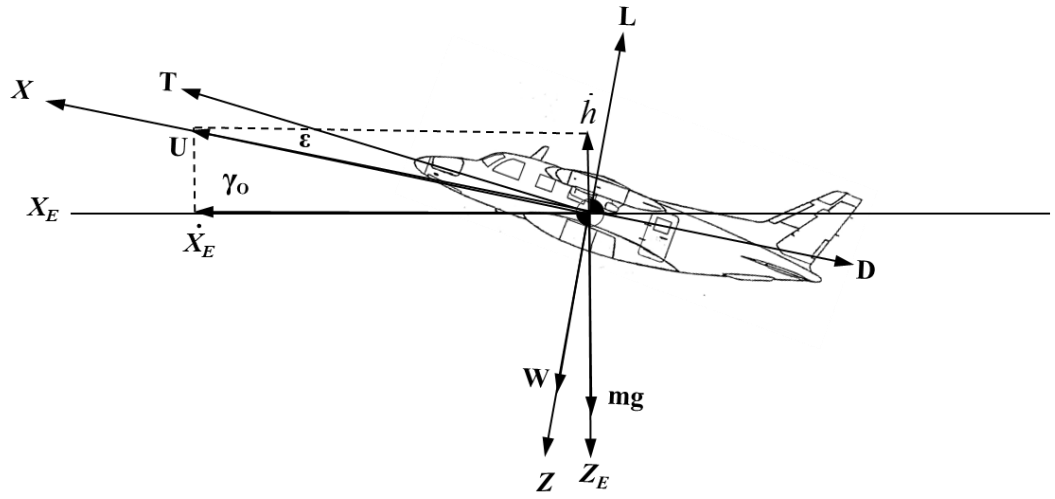

Figure 15. Coordinate system definitions for development of the force equations.

From Figure 15, the equations of motion with respect to the flight path and perpendicular to the flight path may be written using the force distribution on an aircraft during a climb. Resolving the forces in direction parallel and perpendicular to the velocity of aircraft and equating them we get the following two equations

$$T\cos\epsilon + X - mg\sin\gamma_0 = m\dot{U} \tag{1}$$

$$-T\sin\epsilon + Z + mg\cos\gamma_0 = m\dot{W} \tag{2}$$

Where $\varepsilon = \alpha + \phi_T$, we solve $\sin\gamma_0$, we get

$$\sin\gamma_0 = \frac{T\cos\epsilon + X - m\dot{U}}{mg} \tag{3}$$

But here X is the resultant aerodynamic force in the direction of the aircraft velocity and can be replaced with the minus of the Drag (D) force. So we can replace X with $-D$ and the corresponding equation (7) becomes

$$\sin\gamma_0 = \frac{T\cos\epsilon - D - m\dot{U}}{mg} \tag{4}$$

From the figure (19) we can write rate of climb as

$$\dot{h} = U\sin\gamma_0$$

$$\sin\gamma_0 = \frac{\dot{h}}{U} \tag{5}$$

Comparing equation (8) and (9) we get

$$\dot{h} = \frac{U\left(T\cos\epsilon - D - m\dot{U}\right)}{mg} \tag{6}$$

For our case the thrust offset is very small so assuming $\epsilon < 10°$, then the $\cos\epsilon \sim 1$. So we can write

$$\dot{h} = \frac{U\left(T - D - m\dot{U}\right)}{mg}$$

Here $mg = W$ (weight) and solving for drag (D), we get

$$D = T - m\dot{U} - \frac{W\dot{h}}{U} \tag{7}$$

In order to obtain drag we need all other quantities which we will get from the obtained smooth results. We directly have m, W and $\dot{U}$ and all the quantities can be obtained as follows.

Rate of Change of Altitude ($\dot{h}$)

$$\dot{h_n} = \left(\frac{h_{n+1} - h_n}{dt} + \frac{h_n - h_{n-1}}{dt}\right)/2 \tag{8}$$

Here dt is the time period for the given change in altitude. The above equation is for the rate of change of height for all the data points except the first and the last. For the first data point $\dot{h}$ can be obtained as

$$\dot{h_1} = \frac{h_1 - h_2}{dt} \tag{9}$$

And for the last data point

$$\dot{h_n} = \frac{h_{n-1} - h_n}{dt} \tag{10}$$

Flight Test Data Review with Respect to Equation Formulation

Following the development of the data reduction equations, a review of the data flight test data showed that after filtering to remove the noise from the data the data was rather smooth for a period of a second or more. Each flight test was analyzed for variation in the data. A sample of the analysis is shown in Figure 16 below. The mean and standard deviation were evaluated for KIAS Indicated Altitude, Left and Right Torques were examined and found to small deviations from the mean value during periods of interest where data samples were analyzed. The Figure 16 below is a sample of the analysis and is typical of the results. This allowed the equations to simply be reduced to the standard performance form of $T - D = 0$, or $D = T$. This was the form of the equations used in the analysis.

		MU203006	MU203007	MU203009	MU203010	MU203011	MU203012	MU203014	MU203015
KIAS	$\bar{X}$	187	188	189	191	189	194	191	189
	σ	1.7	2.2	1.3	0.7	0.5	0.9	2.7	0.7
H_IND (FT)	$\bar{X}$	9194	9162	9158	9143	9158	9124	9129	10930
	σ	6.3	12.0	11.0	8.0	8.4	5.7	7.2	7.9
TORQUE_L (%)	$\bar{X}$	49.6	50.1	50.4	50.6	53.9	54.4	54.6	51.0
	σ	0.32	0.20	0.15	0.27	0.15	0.13	0.23	0.17
TORQUE_R (%)	$\bar{X}$	50.4	50.0	49.8	50.2	53.8	53.8	54.8	50.5
	σ	0.33	0.27	0.19	0.31	0.22	0.17	0.29	0.20

Figure 16. Review from data of flight test data for stability.

True Air Speed ($\boldsymbol{V_{TAS}}$)

The speed we have in the test results is the Indicated speed and that needs to be converted into True Air Speed (V_{TAS}) and it can be done as follows,

$$V_{TAS}(kt) = V_{KIAS}\sqrt{\frac{\rho_0}{\rho}}$$

$$\therefore V_{TAS}\,(fps) = V_{TAS}(kt) * 1.687 \tag{11}$$

Advance Ratio (J)

The Advance Ratio is a nondimensional coefficient used for propeller charts in order to obtain the efficiency. It is given by the following equation,

$$J = \frac{V_{TAS}}{ND} \tag{12}$$

Here N is the rotation per second of the engine propeller and D is the propeller diameter.

Shaft Horsepower (SHP)

The Shaft Horse Power is given by the following equation,

$$SHP(hp) = percent\ rpm * percent\ torque * rated\ power \tag{13}$$

Here we have percent rpm and percent torque in the test data and we know the rated power of the engine.

Coefficient of Power (C_p)

The Coefficient of Power, C_p, or the propeller is provided by the following equation,

$$C_p = \frac{SHP * 550}{\rho * N^3 * D^5} \tag{14}$$

Propeller Efficiency ($\boldsymbol{\eta_p}$)

Propeller efficiency, η_p, of the engine can be obtained from the table of η_p for the advanced ratio and coefficient of power for the given activity factor.

Thrust (T)

$$T = \frac{\eta_p * SHP * 550}{V_{TAS}} \tag{15}$$

So finally we can substitute all the obtained quantities to find the drag of the aircraft. And from the Drag we can determine the coefficient of drag.

$$C_d = \frac{2D}{\rho V_{TAS}^2 S} \tag{16}$$

And finally from this C_d we can get the increase in C_d because of ice i.e., ΔC_d as follows

$$C_d = C_{d0} + K_i C_l^2 + \Delta C_d$$
$$\therefore \Delta C_d = C_d - C_{d0} - K_i C_l^2 \tag{17}$$

Here the values of C_{d0} and K_i for given test aircraft are 0.0315 and 0.0516 respectively. And the value of C_l can be obtained from equation

$$C_l = \frac{2W}{\rho V_{TAS}^2 S} \tag{18}$$

The sample calculation of this model is shown in Appendix A.

CHAPTER 7 CALIBRATION AND ERROR ANALYSIS

Calibration Flight

Flight test points 1.1 and 1.2 were conducted as pilot familiarization flights and performance analysis. Test point 1.1 was conducted at 15,000 feet pressure altitude, zero-degree C outside air temperature, and a gross weight of 9895 lb. A clean configuration (flaps and gear up) although the aircraft had been fitted with external video cameras and additional flight test instrumentation under the right wing. Propeller RPM was set to 100% which is maximum cruise setting. Test point 1.2 was a performance test with flaps at 20 degrees and a slightly lower gross weight of 9645 lbs.

Test point 1.1

The aircraft was stabilized at 15,000 feet pressure altitude at an indicated airspeed of 230 KIAS. Left and right torques were read and copied into a table. The engine torques were reduced in steps and aircraft was stabilized and torque and airspeed noted. This process was continued for several steps until the airspeed was at 145 KIAS. At this point the engine torques were reduced to 29% and the aircraft allowed to slow to stall.

Test Point 1.2

The test procedure followed the same method as discussed in Test Point 1.1 except the aircraft flaps were deployed to 20 degrees. As the aircraft has a flight limitation to under 155 KIAS with flaps at 20, the initial airspeed was decreased and stabilized to 150 KIAS. The test proceeded as before, noting engine torque and airspeed, reduce torque and stabilize airspeed in small increments until stall.

Flaps down data provides little useful information and was not considered in this analysis.

Calibration Results Test 1.1

The data from Test Point 1.1 were compared to a full three-degree of freedom dynamic model. The computer model's initial conditions were set to the weight, CG, pressure altitude, outside air temperature, and indicated airspeed for each data point taken for test point 1.1. The results of from the computer model was compared to the flight test model (Figure 17). There is very good agreement between the flight test and computer model particularly in the speed range that the tests were conducted, i.e., between 170 and 200 KIAS, with a majority of the flight tests conducted about 190 KIAS.

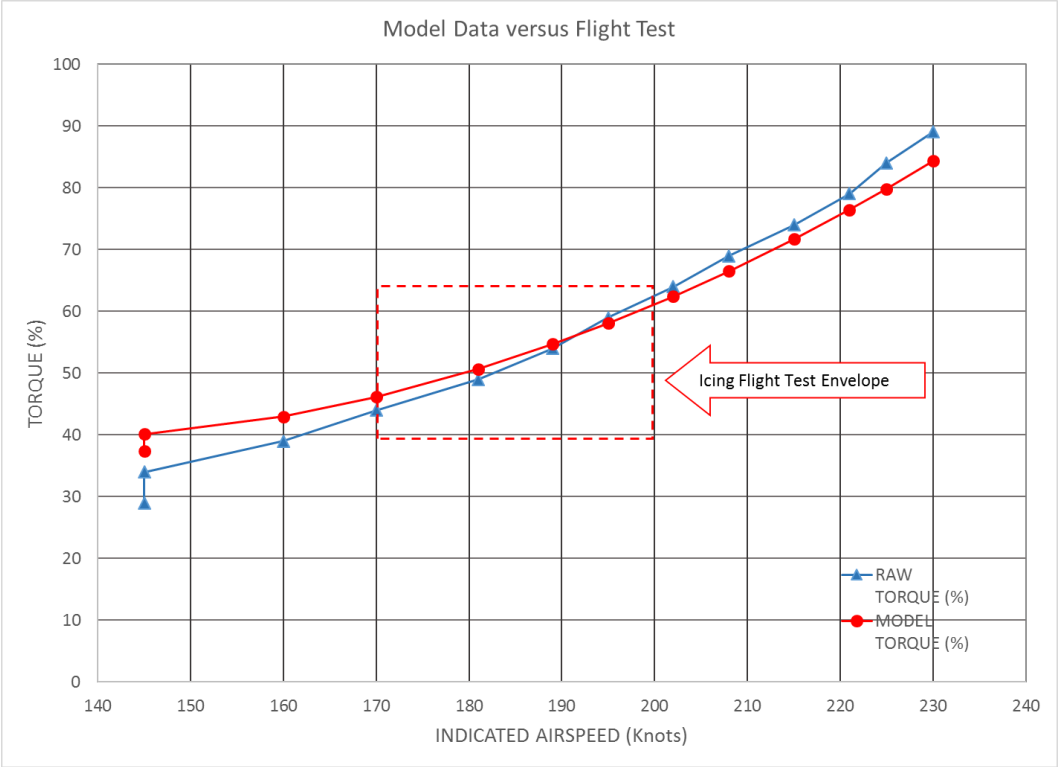

Figure 17. Comparison of flight test data with three degree of freedom model.

Another comparison between the flight test and the computer model was to follow the procedure used to analyze the flight test data to determine the coefficient of drag and compare it with the computer model drag polar. As the weight of the aircraft is known, the lift and thus the coefficient of lift may be directly determined and the drag polars plotted and compared. As the aircraft has power effects and high angles of attack effects, a drag polar in the form of $C_D = C_{D_O} + K_1 C_L + K_i C_L^2$ was chosen as the form to compare.

The results are shown in Figure 18. The variation is not unexpected as the test aircraft has additional equipment installed externally which may account for some variation. That said, the variation in the drag profile was about 1.5% to 5.5% as the aircraft approaches stall and large coefficient of lift. The flight tests were conducted for coefficients of lift between 0.40 and 0.55 with a majority near 0.45.

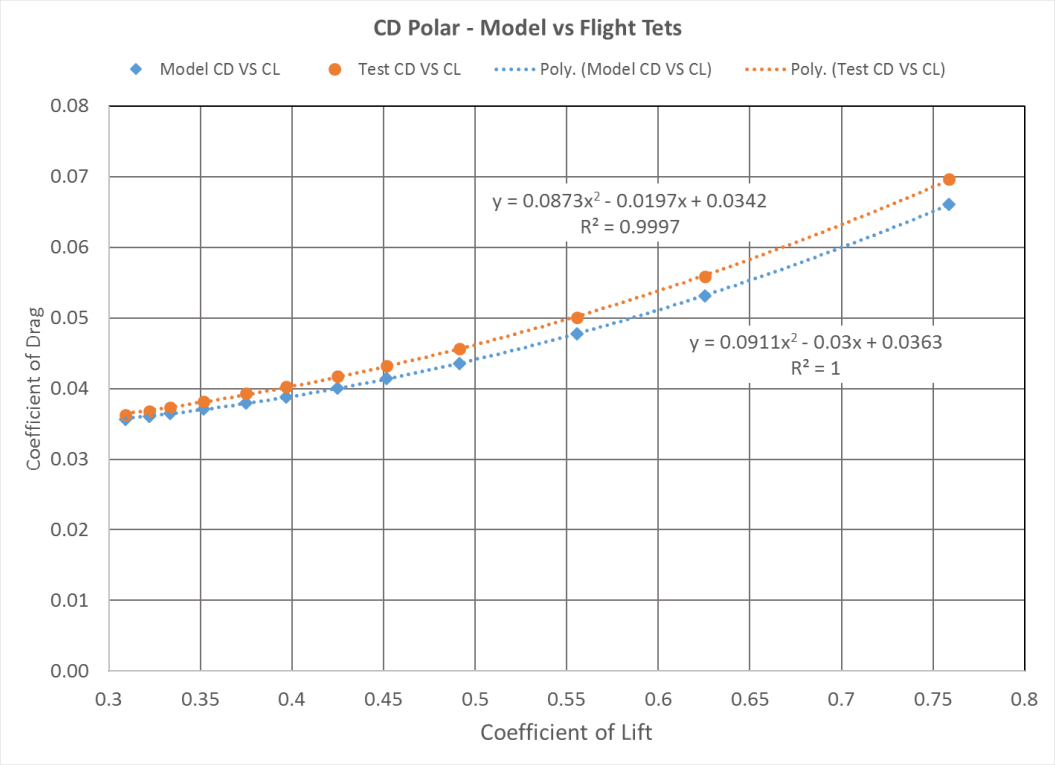

Figure 18. Comparison the drag profiles of the flight test with respect to the three degree of freedom model.

The technique used to calculate the drag from the flight test torque provides a reasonable result. It is known that instrument system on the flight test aircraft has about 2% plus or minus 0.5% error.

Finally, the torques as read by the flight test pilots for a given stabilized flight condition was compared to the computer model. During this test, the data acquisition system was not active and the pilot simply provided the left and right torques along with the indicated aircraft speed. Figure 19 shows the comparison between the model and the flight text data. The difference in the torque data ends up as a difference in the drag between the flight test and computer model as detailed in Figures 17 and 18.

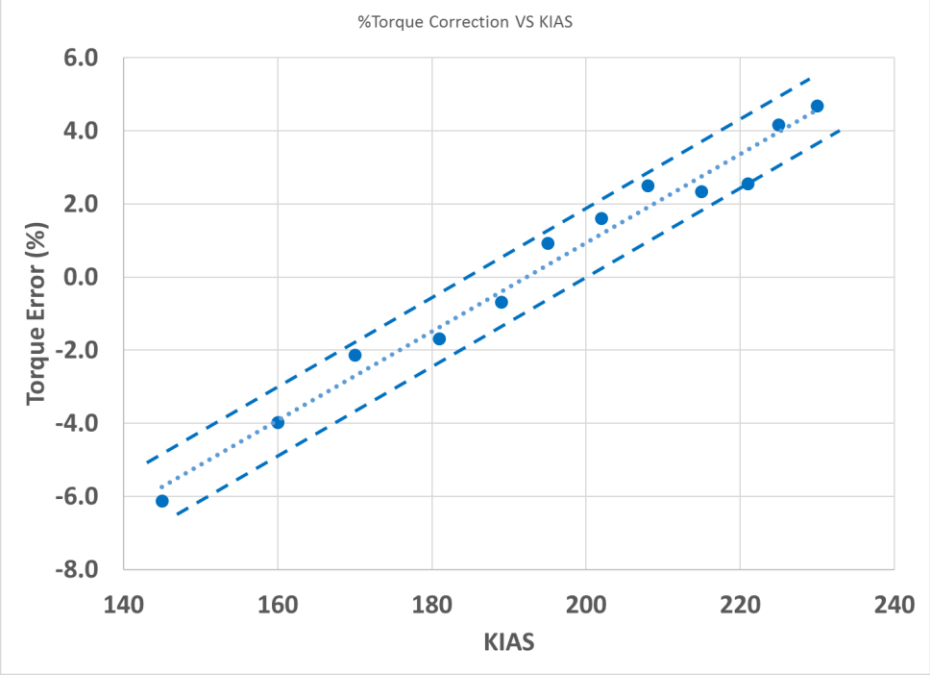

Figure 19. Torque variation between flight test aircraft and model data.

Examination of Test Point 2A, Run 006.

File MU20032A006 was examined and using an approach simplified by assuming the test aircraft attempted and maintained level flight such that the Thrust equaled to drag and the Lift equaled Weight, the fundamental performance equation. The data file was smoothed using a 10-point averaging technique. Figure 20 shows the smoothing of the airspeed data from the data file.

Finally, the drag was calculated from the flight test data using the simplified performance model, again assuming that the test aircraft maintained a straight and level (steady-state) flight condition. The computer model's drag polar of the flight test aircraft was used to calculate the drag coefficient and compared to the flight test aircraft coefficient of drag based on the measured flight test torques. Although the flight test aircraft was flying in very light icing test, most of the ice had sublimated due to the bright sunlight in which the aircraft were flying. This is only important in noting that the drag due to icing for this case should be low and Figure 21 shows the result.

The result of this example shows the coefficient of drag calculated using the flight test aircraft and model data practically overlap one another with nearly zero difference, an average of -0.0001 with a standard deviation

of 0.0006. This works out to be a variation of about 1.3 percent in coefficient of drag.

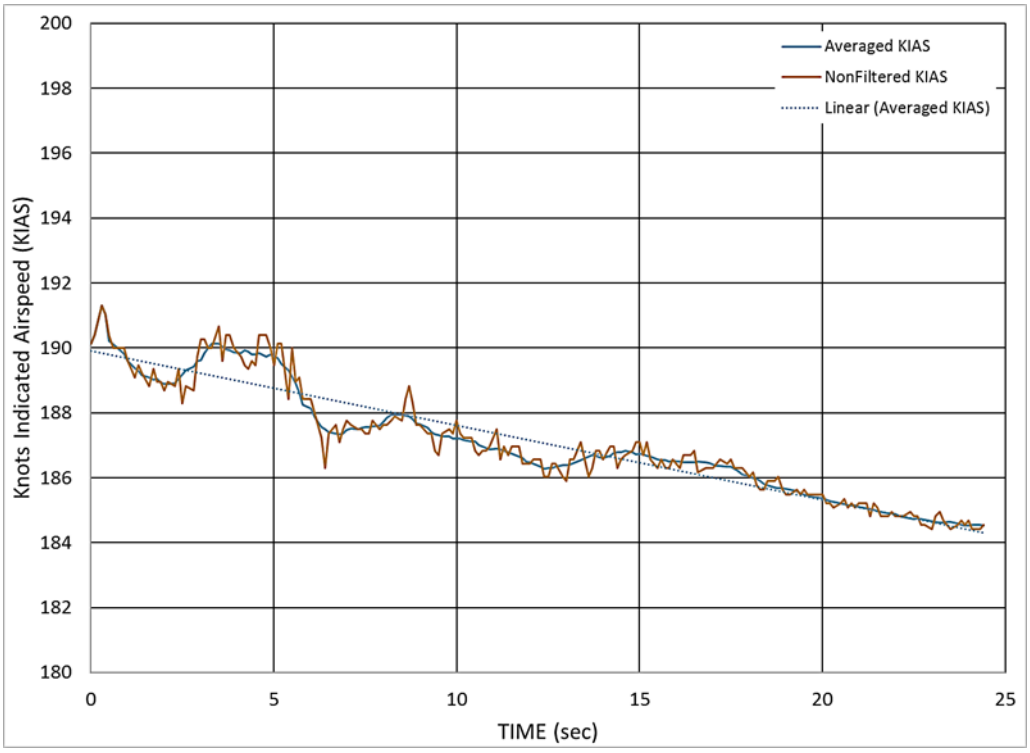

Figure 20. Ten-point averaging of the indicated airspeed.

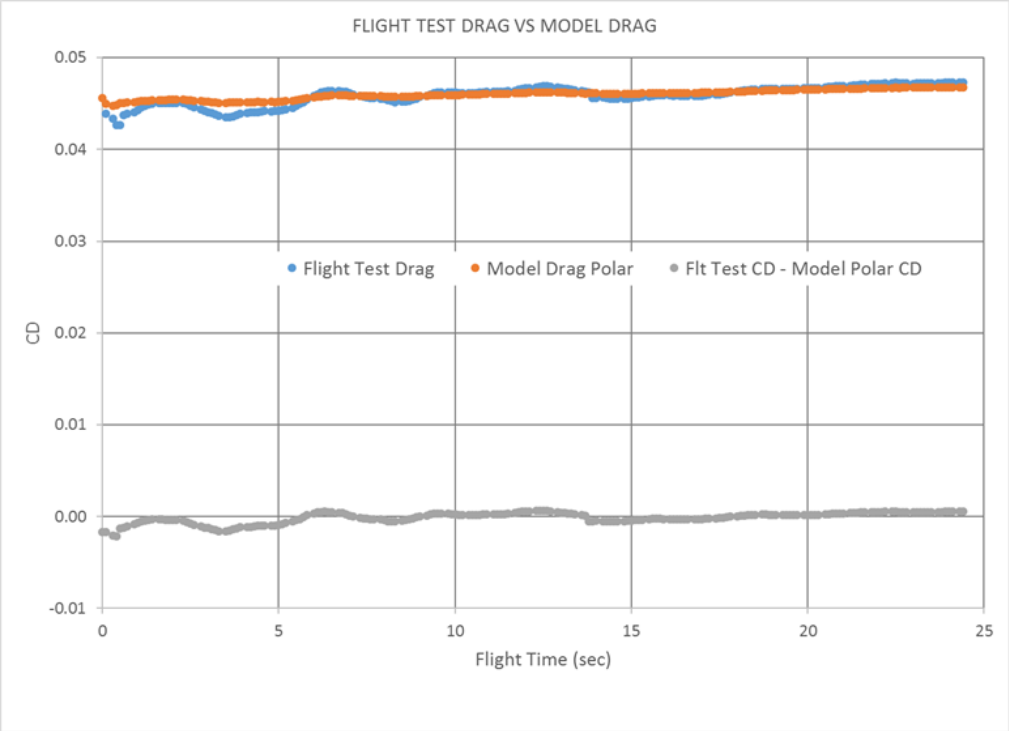

Figure 21. Comparison of drag coefficient between model drag profile and torque derived drag profile.

CHAPTER 7 RESULTS

The flight tests were carried out at different altitudes and flight speed with different values of MVD and LWC. The test points executed are shown in Figure 6a and 6b. The data files associated with the test points are provided in Table 3. Flaps 20 data was not evaluated in this analysis.

Analysis of a Data File without a Boot Activation Shown in Data

Velocity Variation

Flight test condition 4A, Run 014, as shown in Table 3, is used to demonstrate the analysis process in determining the coefficient of drag of the aircraft. It this case the test aircraft entered the icing cloud, accumulates a specific level of ice on the horizontal stabilizer. Once the level of icing had been achieved the test aircraft left the airstream, stabilized its flight condition and activated the anti-icing system – a pneumatic boot system on the main wings, horizontal and vertical stabilizers. Although the data acquisition system was operating throughout the flight, File MU20044A014A only contains 43.9 seconds of data which began after the pneumatic boot had been activated.

TABLE 3. FLIGHT TEST DATA FILES ASSOCIATES WITH THE FLIGHT TEST CARD

			TIME WINDOW											
FILE NAME	TEST CARD POINT	RUN NUMBER	START TIME (ZULU)	FILE LENGTH (SEC)	PRESSURE ALTITUDE (FT)	INDICATED AIRSPEED (KIAS)	AIRFRAME CONFIGURATION	TOTAL AIR TEMP (DEG C)	AIRCRAFT WEIGHT (LBS)	CG (FS) (INCHES)	LWC (g/m^3)	MVD (uM)	ICE CLOUD AIR TEMP (DEG C)	Notes
MU20032A006A	2A	006A	19:01:22	24.4	9201	190	CLEAN	1.7	11090	196.59	0.15	23	-4	
MU20032A007A	2A	007A	19:17:19	26.2	9169	185	CLEAN	2.7	10915	196.64	0.15	23	-4	
MU20032A009F	2A	009F	19:19:29	24.4	9168	187	CLEAN	3.0	10882	196.64	0.15	23	-4	
MU20032A010A	2A	010A	19:20:51	18.7	9144	191	CLEAN	2.7	10875	196.65	0.15	23	-5	
MU20032A011A	2A	011A	19:32:31	15.2	9152	190	CLEAN	2.7	10760	196.66	0.15	23	-5	
MU20032A012A	2A	012A	19:49:11	25.2	9127	195	CLEAN	3.1	10574	196.67	0.15	23	-5	
MU20032A014A	2A	014A	19:53:33	130.2	9133	190	CLEAN	3.9	10513	196.67	0.15	23	-5	
MU20032A015A	2A	015A	19:53:33	38.3	10929	188	CLEAN	-1.1	10436	196.68	0.15	23	-5	2 Boot Actuations
MU20044A004A	4A	004A	18:14:44	62.5	10373	185	CLEAN	0.0	10823	196.65	0.64	34	-6	
MU20044A005A	4A	005A	18:16:40+	50.7	10369	189	CLEAN	-0.1	10808	196.66	0.64	34	-6	
MU20044A006A	4A	006A	18:30:43	46.8	10380	185	CLEAN	-0.2	10661	196.67	0.64	34	-6	
MU20044A007A	4A	007A	18:32:55	73.9	10370	188	CLEAN	0.5	10636	196.67	0.64	34	-6	1 Boot Actuation
MU20044A008A	4A	008A	18:41:15+	49.0	10858	187	CLEAN	-1.0	10549	196.67	0.64	34	-6	
MU20044A009A	4A	009A	18:56:26	162.5	10861	183	CLEAN	-0.6	10390	196.60	0.64	34	-6	1 Boot Actuaction
MU20044A010A	4A	010A	19:09:23	52.4	10858	189	CLEAN	0.0	10254	196.61	0.47	51	-6	
MU20044A011A	4A	011A	19:30:24	161.7	10870	177	CLEAN	-0.8	10018	196.50	0.47	51	-6	2 Boot Actuations
MU20044A012A	4A	012A	19:43:30	80.7	11276	189	CLEAN	-0.8	9877	196.39	0.41	36	-7	
MU20044A014A	4A	014A	20:10:27	43.9	11316	176	CLEAN	-1.6	9581	196.14	0.41	36	-7	
MU20044A015A	4A	015A	20:13:44	153.6	11318	176	CLEAN	-1.7	9561	196.12	0.41	36	-7	1 Boot Actuation
MU20048C016A	8C	016A	20:26:22	52.6	11375	151	FLAPS 20	-3.2	9426	196.00	0.18	22	-6	
MU20048C017A	8C	017A	20:45:40	128.0	11298	149	FLAPS 20	-3.1	9232	195.82	0.18	22	-6	1 Boot Actuation
MU20057B006A	7B	006A	19:31:23	75.3	10295	179	CLEAN	0.5	11147	196.57	0.65	48	-5	
MU20057B007A	7B	007A	19:45:15+	204.2	10275	173	CLEAN	0.3	11006	196.61	0.65	48	-5	1 Boot Actuation
MU20057B008A	7B	008A	20:12:30	118.7	10109	168	CLEAN	-0.5	10695	196.67	0.65	48	-5	1 Boot Actuation
MU20057B009A	7B	009A	20:32:29	70.2	10298	168	CLEAN	-0.6	10496	196.67	0.77	40	-5	
MU20057B010A	7B	010A	20:51:16	39.2	10181	163	CLEAN	-0.9	10305	196.63	0.77	40	-5	1 Boot Actuation
MU20057B011A	7B	011A	20:52:57	72.1	10207	164	CLEAN	0.0	10273	196.62	0.77	40	-5	
MU20057B013A	7B	013A	21:07:46	94.0	10176	163	CLEAN	0.6	10121	196.55	0.77	40	-5	
MU20057B015A	7B	015A	21:33:30	50.4	10267	162	CLEAN	0.2	9856	196.37	0.77	40	-5	
MU2005AC016A	10C	016A	21:21:36	58.8	10266	150	FLAPS 20	-1.4	9824	196.35	0.77	40	-5	
MU2005AC018A	10C	018A	21:52:59	169.2	10302	147	FLAPS 20	-2.5	9661	196.21	0.71	29	-6	1 Boot Actuation
MU2005AC019A	10C	019A	22:19:26	170.3	10312	141	FLAPS 20	-2.2	9405	195.98	0.39	26	-5	1 Boot Actuation
MU20067B012A	7B	012A	20:22:43	72.3	10597	163	CLEAN	0.1	10638	196.67	0.78	64	-5	
MU20067B013A	7B	013A	20:30:36	149.8	10680	156	CLEAN	-1.1	10561	196.67	0.78	64	-5	1 Boot Actuaction
MU20067B014A	7B	014A	20:42:53	127.4	10760	157	CLEAN	-0.8	10435	196.68	0.78	64	-5	1 Boot Actuation
MU20067B015A	7B	015A	21:04:00	130.7	10535	157	CLEAN	-0.4	10225	196.60	0.56	55	-4	1 Boot Actuation
MU20067B016A	7B	016A	21:32:26	83.6	10169	159	CLEAN	0.3	9948	196.45	0.56	54	-4	1 Boot Actuation
MU20067B017A	7B	017A	21:37:35	75.8	10150	179	CLEAN	1.8	9892	196.4	0.56	54	-4	

The raw data (non-processed data) from the file was passed through the non-phase shifting, fifth-order Butterworth filter to reduce data noise while maintaining proper phase between the various variables in the data file. As an example, Figure 22 shows the variation of the air speed with time with the blue line being the indicated airspeed prior to filtering and the orange line being the filtered indicated airspeed. Note that the two curves are overlapping with minimum phase difference. The data in the file are taken after the desired ice accumulation is achieved.

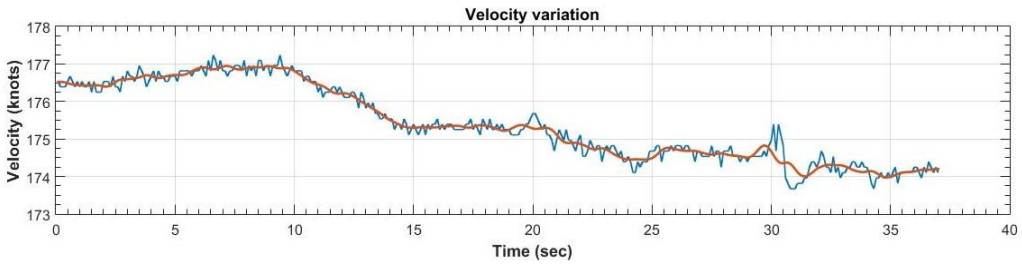

Figure 22. Filtered indicated airspeed compared to base airspeed with respect variation with respect to time.

Percent Torque

Figure 23 compares the post ice accumulation flight test aircraft engine torque to a theoretical clean aircraft torque for the same flight condition. The theoretical aircraft model was calibrated against the flight test aircraft as described in Chapter 7. We can see in Figure 21 that there is almost little variation (less than 0.3%) in the torque throughout the data

period. This variation is within the measurement error of the instrumentation system.

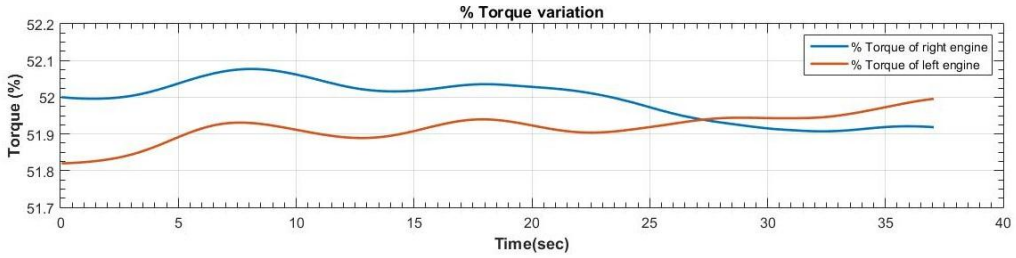

Figure 23. Percent torque variation with time due to icing

.

Percent RPM of Left Engine

Figure 24 shows that the RPM maintains a 100 percent value as it should. The variation is within measurement error.

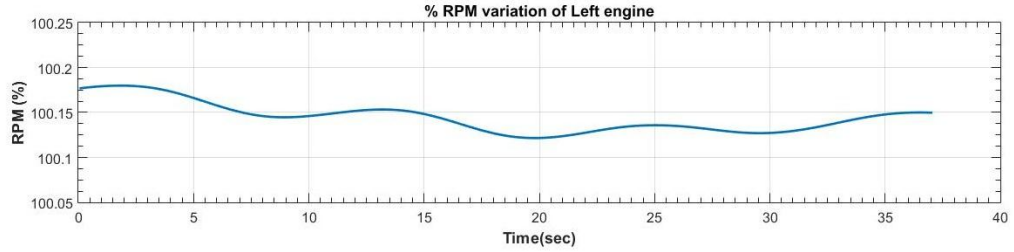

Figure 24. Percent RPM variation of left engine.

Coefficient of Drag

The coefficients of drag for the “iced” flight test aircraft and the baseline “non-iced” model were determined using the process developed in Chapter 6. Figure 25 shows the flight test airspeed as a function of time. This airspeed was used along with the other flight conditions to determine

the coefficient of drag for the flight test vehicle and for the base line clean aircraft model. The coefficient of drag for both are plotted together so the iced-aircraft's coefficient of drag could be compared to the clean aircraft model.

A comparison of the coefficient of drags in Figure 25 shows that the flight test aircraft had an increased drag coefficient of about 0.009-0.01 above the clean aircraft model. This is about 21.6% increase due to ice accumulation on the flight test vehicle.

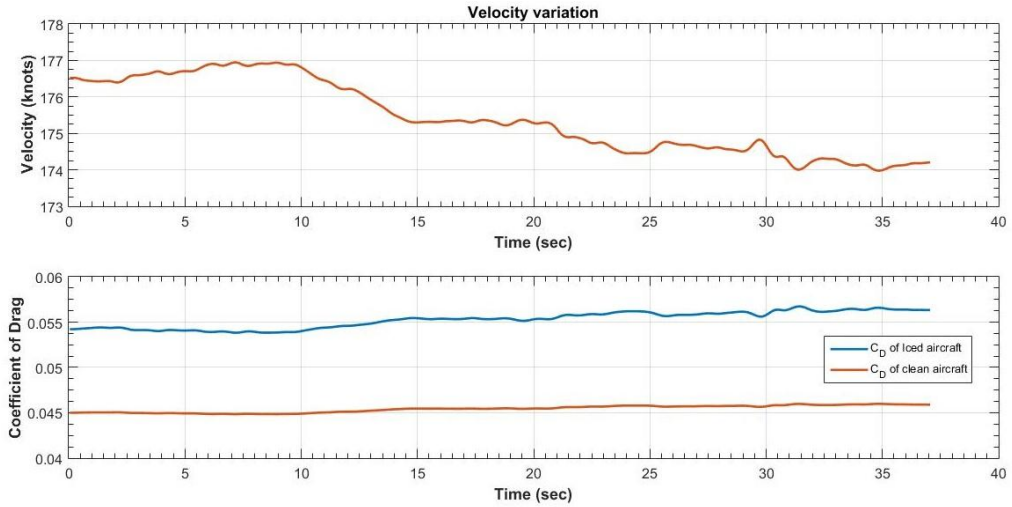

Figure 25. Coefficient of drag variation with time due to icing.

Analysis of a Data Fill with a Boot Actuation

Velocity Variation

The flight test condition is shown in TABLE 4 file name MU20067B015A. The test aircraft was flying at 157 KIAS at a pressure

altitude of 10535 ft. in a clean configuration. The icing cloud had an average liquid water content of 0.56 g/m^3 with a median volumetric diameter of 55 microns. The temperature was -4 C.

The Figure 26 shows the variation of the air speed with time. Prior to boot activation, the test aircraft flew in station keeping mode in order to maintain the cloud stream down the left side of the aircraft in order to accumulate ice to a prescribed height. Once the ice had been accumulated the test aircraft exited the cloud stream and stabilized the flight condition to the prescribed airspeed for the test. Then the pilot activates the pneumatic boot and the ice is shed from the flight surface. Residual ice may remain on the aircraft behind the boots or on non-protected surfaces. Without changing the engine torque the aircraft performance is evaluated for change in airspeed and trim. For this case after the boot was actuated, the airspeed increases suggesting that the drag due to ice accumulation was significant. Although the pilot does not apply additional torque, the torque will increase as airspeed increases.

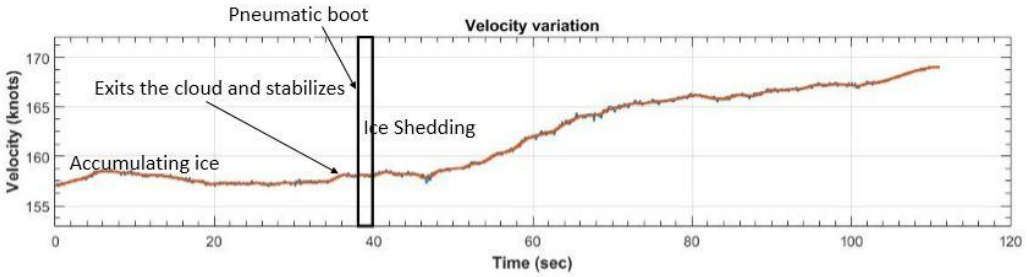

Figure 26. Air speed variation with time.

Percent Torque of Engines

We can see in Figure 27 that there is almost no change (max 1%) in the torque throughout the flight. The rise in the end is the manual command by the pilot.

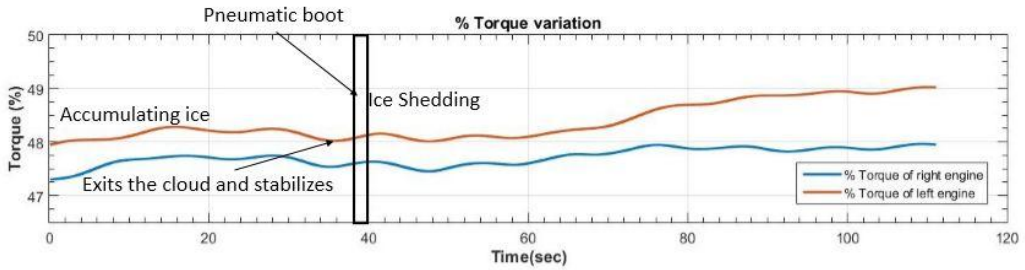

Figure 27. Torque variation with time

Coefficient of Drag

Figure 28 compares the coefficient of drag calculated from the flight test data to that of the baseline model. The comparison shows a period prior to boot activation where the flight test aircraft drag is increasing when compared to the “clean” aircraft model. The flight test aircraft is in the icing

cloud and accumulating ice on its control surfaces and airframe and drag is increasing. Once the test aircraft pneumatic boots are activated and ice is shed, drag decrease and the airspeed increases without pilot intervention to increase airspeed. The red line is for the clean aircraft so we can also see the increase in coefficient drag because of icing.

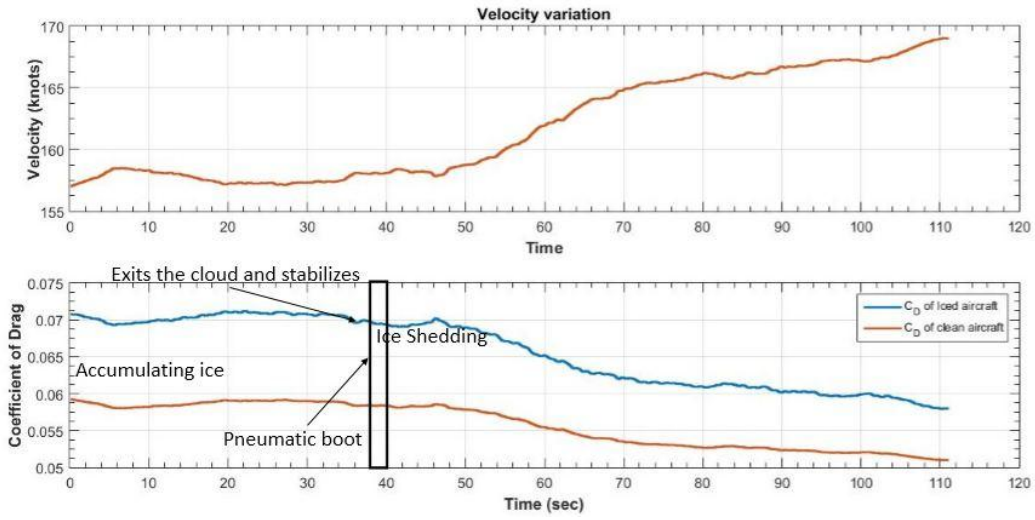

Figure 28. Variation and comparison of Coefficient of Drag.

If we calculate the coefficient of drag for both cases, then we get overall about 17.72% increase in coefficient of drag and ultimately drag.

Results of Analysis for All Clean Configurations

Out of 33 test files following Table 4 shows the important file showing the increase in drag. And from this table we can see that the max increase in drag is 22.9% and with the average of 6.6% increase. From this we can imagine that the 2/3rd part of tail plane icing on just left side can cause such

high increase in drag then the icing of both side can cause severe drag increase. And all the graph of variation of coefficient of drag of all the files are shown and compared in figures of Appendix.

Plotting the graph of percent increase in drag versus the Liquid water content and Mean Volumetric Diameter respectively we get the results as shown in Figures 29 and 30. Here different coloured dots belong to different flight conditions.

TABLE 4 MAXIMUM DIFFERENCE BETWEEN CALCULATED FLIGHT TEST DRAG COEFFICIENT AND THE BASELINE MODEL.

File name	Liquid Water Content, LWC (gm/cubic m)	Median Volumetric Diameter MVD (μM)	CD	CD Model	% Change
203006	0.15	23	0.0455	0.0426	6.8
203007	0.15	23	0.0449	0.0451	-0.5*
203009	0.15	23	0.0444	0.0448	-0.8*
203010	0.15	23	0.0429	0.0439	-2.3*
203011	0.15	23	0.0474	0.0442	7.1
203012	0.15	23	0.0444	0.0424	4.7
203014	0.15	23	0.0472	0.0432	9.1
203015	0.15	23	0.0434	0.0434	0.2
204004	0.64	34	0.0475	0.0456	4.1
204005	0.64	34	0.0449	0.0442	1.7
204006	0.64	34	0.0471	0.045	4.6
204007	0.64	34	0.0466	0.0448	4.1
204008	0.64	34	0.0458	0.0442	3.6
204009	0.64	34	0.0485	0.0449	8.0
204010	0.47	51	0.0449	0.0431	4.3
204011	0.47	51	0.0509	0.0446	14.1
204012	0.41	36	0.0444	0.0419	6.0
204014	0.41	36	0.0553	0.0454	21.6
204015	0.41	36	0.0498	0.043	15.9
205006	0.65	48	0.0495	0.051	-2.9*
205007	0.65	48	0.0521	0.0516	0.9
205008	0.65	48	0.0615	0.0553	11.2
205009	0.77	40	0.0556	0.0525	6.0
205010	0.77	40	0.0652	0.0578	12.8
205011	0.77	40	0.0588	0.0549	7.1
205013	0.77	40	0.0629	0.0558	12.6
205015	0.77	40	0.0556	0.0542	2.7
206012	0.78	64	0.0541	0.0576	-6.1*
206013	0.78	64	0.0649	0.0648	0.12
206014	0.78	64	0.0623	0.0576	8.1
206015	0.56	55	0.0656	0.0557	17.7
206016	0.56	54	0.0682	0.0555	22.9
206017	0.56	54	0.0487	0.0449	8.4

*Negative drag is a result of using the aircraft model as a baseline and is a reflection of the differences torque and drag profiles as noted above.

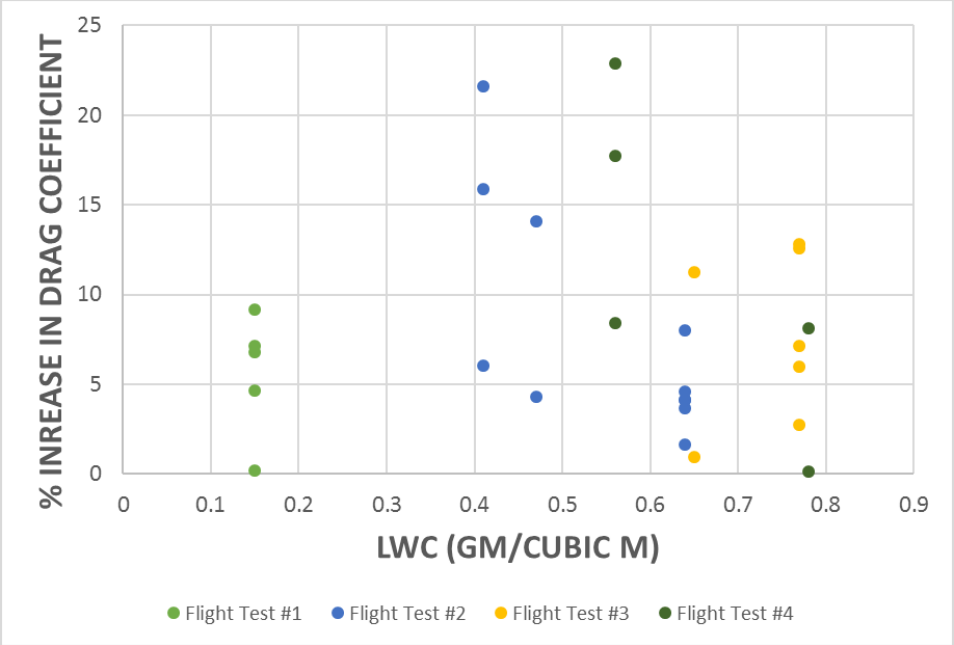

Figure 29. Percent increase in drag v/s Liquid Water Content.

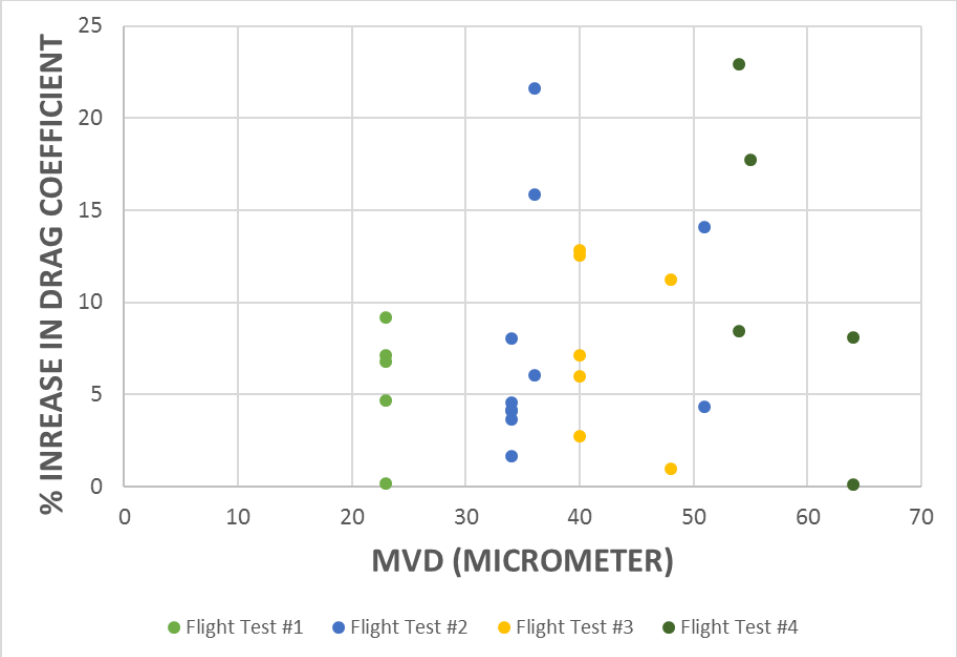

Figure 30. Percent increase in drag v/s Mean Volumetric Diameter.

CHAPTER 8

CONCLUSION

The data reduction of the aircraft flight test data showed that certain icing conditions could significantly increase the drag on the aircraft. As only the left-side of the aircraft was involved in the icing cloud during the ice accretion event it would appear that full evolvement of the aircraft would more than double the drag encountered.

The method chosen to review and compare the flight test data provided adequate information to estimate drag increase when an aircraft is properly instrumented and a baseline determined and set based on a flight test calibration test and a computer model of the aircraft.

For this particular flight test, there are a few specific results of note and should be considered when discussing the analytic results.

- There is almost no increase in the coefficient of drag for smaller values of the Liquid Water Content and smaller values of Median Volumetric Diameter.
- There is a significant increase in the coefficient of drag the higher values of the Liquid Water Content and higher values of the Median Volumetric Diameter. For our case we get higher Coefficient of drag from the Liquid Water Content of 0.41 $\mathrm{gm/m^3}$ and from the Median Volumetric Diameter of 34 $\mu\mathrm{m}$ of the water droplet.

- Only a portion of the left-side of the test aircraft was in the icing cloud and was only about 1/3rd of the total aircraft surface area results in about 13.5% increase in drag and so the effect will be severe in case of icing on both side.
- Issues with the flight test was the lack of cloud cover to shield the aircraft as it would be in icing encounters. The sun was bright and shown on the black, pneumatic boot adding a radiance transfer that may speculatively account for some of the self-shedding that occurred during testing. In addition, a pre- and post- test flight calibration would have provided better test aircraft calibration data especially for the 2000 to 3000 pound changes in weight that occurred on each day's flight test.

CHAPTER 9

FUTURE WORK

This work allowed the estimation of drag from a flight test. These types of studies are very expensive and allow only a limited set of data to be taken during a testing period. In addition, the types of facilities available for these tests are difficult to find due to the reduction in available equipment as government agencies retire or reduce equipment.

In order to move to the next step, it is suggested that computer codes that have been developed to specifically study airframe icing be employed to first recreate this flight test to compare the results of this work with a model. Secondly, to expand the study to include the full model of the test aircraft to examine the effect of the icing levels in this work to the change in not only drag, but lift and pitching moment. Of particular interest is a computer code developed by Dr, Wagni Habashi and his team at Newmerical Technologies International. Recently, ANSYS acquired the rights to FENSAP-ICE. Information may be found at the references below.

- http://www.ansys.com/Products/Fluids/ANSYS-FENSAP-ICE
- http://www.ansys.com/Products/Fluids/Simulating-Aircraft-Icing

REFERENCES

[1]Petty, Kevin R., and Floyd, Carol D. J., "A statistical Review of Aviation Airframe Icing Accidents in the US," American Meteorological Society, Paper 8142

[2]Jeck, R.K., "A New Data Base of Supercooled Cloud Variables for Altitudes up to 10,000 Feet AGL and Implications flr Low Altitude Aircraft Icing," DOT/FAA/CT-83/21, FAA Technical Center, Atlantic City Airport, NJ, 1983.

[3]Trunov, O. K., and Ingleman-Sundberg, M., "On the Problem of Horizontal Tail Stall Due to Ice," *A joint report from the Swedish Soviet working group on Scientific- Technical cooperation in the field of flight safety*, Report No. JR-3, 1985.

[4] Ruff, G. A., "User's Manual for the NASA Lewis Ice Accretion Prediction Code (LEWICE)," Sverdrup Corp., Middleburg Heights, OH, April 1988.

[5]Griffiths, R. C., and Korkan, K. D., "Application of Pneumatic De-ice Boots for Leading Edge Ice Accretions Utilizing LEWICE - A Summary," SAE/ AHS Aircraft Icing Technology Workshop, Cleveland, OH, September 21-22, 1992.

[6]Smith, D., Mullins, Jr., and Korkan, K., "Effects of Icing on the Aerodynamic Performance of a Series of Two-Dimensional Airfoils at Low Reynolds Number," AIAA 95-0453, 33rd Aerospace Sciences Meeting and Exhibit, Reno, NV, January 9-12, 1995.

[7]Mullins, Jr., Smith, D., and Korkan, K., “Effects of Icing on the Aerodynamic Performance of a Flapped Airfoil,” AIAA 95-0449, 33rd Aerospace Sciences Meeting and Exhibit, Reno, NV, January 9-12, 1995.

[8]Ferguson, S.W., Mullins, B.R., Smith, D.E., and Korkan, K.D. “Full-Scale Empennage Wind Tunnel Test to Evaluate Effects of Simulated Ice on Aerodynamic Characteristics,” AIAA 95-0451, 33rd Aerospace Sciences Meeting and Exhibit, Reno, NV, January 9-12, 1995

[9]Ashenden, Russell, “In-flight Icing Test Plan,” EAFB, 412th Test Wing, EAFB, CA, 4 DEC 1992

[10]Ashenden, Russel A., “The Air Force Flight Center Artificial Icing and Rain Testing Capability Upgrade Program,” 33rd Aerospace Sciences Meeting and Exhibit, 1995, 10.2514/6.1995-450,

[11]Ashenden, Russell, Conducting Artificial Tailplane Icing Evaluations at the Air Force Flight Test Center,” AIAA 95-0450, 33rd Aerospace Science Meeting and Exhibit, January 9-12, 1995, Reno, NV.

[12]Ashenden, R. A., “MU-2B-60 IN-FLIGHT ICING TEST, Report No. C9300100, 445th Test Squadron, 04 FEB 93.

[13]ANON, “System/360 Scientific Subroutine Packages, (360A-CM-03X) Version III,” Programmer’s Manual, IBM Corp, White Plains, NY, 1968.

[14]Oppenheim, A.L., and Schafer, R.W., “Digital Signal Processing,” Prentice-Hall, Inc., Englewood, NJ, 1975.

[15]Fairchild, Jack E., “Notes on Fundamentals of Flight Mechanics,” The University of Texas at Arlington, 1987.

APPINDIX

SAMPLE CALCULATIONS

The calculation of all the above quantities for one of my case is as follows

$$h_1 = \frac{10538.203 - 10538.104}{0.1} = 0.9949$$

$$\dot{U} = 0.079711$$

$$W = 10225\ lb$$

$$g = 32.17\ ft/sec^2$$

$$m = \frac{W}{g} = 317.82\ lb$$

$$V_{KIAS} = 157\ kts$$

$$V_{TAS} = 157 * \sqrt{\frac{0.002377}{0.0017}} = 186.205 = 314.13\ fps$$

$$N = 1.0038 * \frac{1591}{60} = 26.62\ rps$$

$$D = 8.1667\ ft$$

For left engine

$$J_L = \frac{V_{TAS}}{ND} = \frac{314.127}{26.62 * 8.1667} = 1.445$$

$$SHP_L = 1.0038 * 0.47843 * 715 = 343.3773\ hp$$

$$C_{pL} = \frac{343.3773 * 550}{0.0017 * 26.62^3 * 8.1667^5} = 0.163$$

The Activity factor of our test plane propeller is 123 and for the obtained value of J and C_p from the table the propeller efficiency (η_p) is 84.7%.

Now Thrust

$$T_L = \frac{0.847 * 343.3773 * 550}{314.1274} = 509.23\ lb$$

Similarly, for right engine

$$J_R = \frac{V_{TAS}}{ND} = \frac{314.127}{26.62 * 8.1667} = 1.448$$

$$SHP_R = 1.0038 * 0.4703 * 715 = 336.697\ hp$$

$$C_{pR} = \frac{343.3773 * 550}{0.0017 * 26.62^3 * 8.1667^5} = 0.161$$

The value of propeller efficiency is almost same i.e. 84.7%

$$T_R = \frac{0.847 * 336.697 * 550}{314.1274} = 499.32\ lb$$

Now Drag

$$D = 1118.2\ lb$$

$$C_d = 0.0749$$

$$C_{d,Clean\ aircraft} = 0.0558$$

$$\Delta C_d = 0.0191$$

This entire calculation is coded in MATLAB® for all the cases.

BIOGRAPHICAL INFORMATION

Shehzad M. Shaikh was born on November 5th, 1990 in Navsari of Gujarat state in India to his mother Mumtaz M. Shaikh and father Maksudahmad Y. Shaikh. He attended the elementary education at Vidyakunj English medium school. Right from his school days he was very much passionate about the spacecraft, aircraft, satellites etc. and hence he decided to pursue a career in the Aerospace engineering. He earned his bachelor's degree in Aeronautical Engineering from Sardar Vallabhbhai Patel Institute of Technology in India and master's degree from University of Texas at Arlington.

While the college ambience at the Sardar Vallabhai Patel Institute of Technology and at University of Texas at Arlington, did much to strengthen his resolve as well as motivate him, He felt drawn towards projects and presentations the most making him an enthusiastic and energetic participant in several paper presentations, seminars, workshops and projects. Goal oriented and focused, theoretical frameworks in Mathematics and Sciences, which drive the physical world, always interested him. This facilitated him in setting a solid foundation of fundamentals and strengthening his basics. Creative instincts, excellent fellowman ship and perceptiveness became his mentors. His endeavor to learn the latest technology has been a great motivator and it continuously prompted him to

keep moving to gain additional knowledge from various sources to add to his own courseware. His research interest is in the aerodynamics, design, helicopter and its dynamics, icing and orbital mechanics and it can be seen in his academic career and projects. Among his accomplishments, apart from this thesis, are two noteworthy projects namely, “Experimental Analysis of Wind Rotor Blade With and Without Vortex Generators” accomplished under the company Suzlon Energy Limited. In this project the detailed analysis of the blade for optimum aerodynamic performance by implementing Vortex Generators was carried out in the wind tunnel. The second project was “Anti-Torque and Yaw Control System for Helicopters Using Circulation Control Technique (Notar Configuration)” based on Numerical analysis of the tail boom of helicopters. The detailed analysis of the tail boom for optimum aerodynamic performance by implementing Coanda slots was carried out in ANSYS software. The success was such that publishing these projects in national Level Journals was strongly recommended. The project list don’t stop here it goes on and on.

Mr. Shaikh received a good exposure in aaerospace engineering and he desires to be a research engineer to fathom more depth of the his passion.